Nonlinear Dyn (2021) 106:1975–2003
https://doi.org/10.1007/s11071-021-06889-z

ORIGINAL PAPER

Flutter control and mitigation of limit cycle oscillations in aircraft wings using distributed vibration absorbers

Ehab Basta · Mehdi Ghommem · Samir Emam

Received: 12 April 2021 / Accepted: 3 September 2021 / Published online: 19 October 2021

Abstract In this work, we demonstrate the application of the conserved-mass metamaterial concept to control the flutter onset in aircraft wings and mitigate their induced vibrations. The numerical study is conducted on a rigid airfoil that is supported by nonlinear springs in the pitch and plunge directions and subjected to nonlinear aerodynamic loads. The aeroelastic system is attached to an array of passive vibration absorbers. The mass of the vibration absorbers is deducted from the mass of the aeroelastic structure, which makes the total mass of the system conserved. The equal mass constraint is imposed so that improvements in the aeroelastic performance are due to the addition of the vibration absorbers and not the added mass attached to the main aeroelastic system. The linear analysis of the aeroelastic system reveals that a proper selection of the stiffness and position of the vibration absorber leads to 23.4% increase in the flutter speed when deploying one single absorber. Placing the vibration absorber closer to the leading edge is observed to delay the occurrence of flutter. Furthermore, considering an array of distributed vibration absorbers with a proper selection of their stiffness is found to result in an increase of the flutter speed by 84%. We also develop the normal form of the aeroelastic system equipped with the vibration absorber using the method of multiple scales to investigate the limit cycle oscillations (LCOs) beyond the flutter boundary (Hopf bifurcation). The analytical results are verified against their numerical counterparts. The normal form is used to examine the effects of the vibration absorber stiffness nonlinearities on the dynamic behavior of the aeroelastic system. Incorporating quadratic and cubic stiffness coefficients is found to degrade the aeroelastic system by amplifying the amplitude of LCOs beyond flutter. However, soft pitch spring proved to be beneficial to decrease the LCO amplitude. Moreover, the increase in the number of the vibration absorbers while imposing the equal mass constraint is observed to lead to relatively lower LCO amplitudes in the post-flutter regime.

Keywords Aircraft wings · Flutter suppression · Conserved-mass metastructure · Passive vibration absorber · Normal form

E. Basta · M. Ghommem (✉) · S. Emam
Department of Mechanical Engineering, American University of Sharjah, Sharjah 26666, UAE
e-mail: mghommem@aus.edu

1 Introduction

Two-dimensional rigid airfoil undergoing pitch and plunge motions has been commonly used to gain insights on the nonlinear dynamic behavior of aeroelastic systems [1–4]. Aerodynamic structures with airfoil sections have been applied to several

engineering systems [6–8]. The wings of airplanes, the blades of compressors and wind turbines all contain elements with airfoil cross sections. The coupled dynamic interaction of the airfoil section with the airstream is a crucial element in the design of aeroelastic systems. For wind turbines, researchers sought to maximize the harvested energy from the wind [9]. While an increase in the rotational speed of the wind turbines may seem to enhance the performance of the system, the amplitude of vibration of the constituting blades may damage the structure. The same concerns are extended to aircraft designs [10]. The high speed of a flying aircraft can result in the large-amplitude vibrations of wings due to the aerodynamic loads. Thus, for a safe flight operation, the maximum speed of aircraft is restricted to avoid any large amplitude of vibrations. In dynamic aeroelasticity, this phenomenon is referred as to flutter. Flutter is a potentially damaging phenomenon which may take place in flexible structures subjected to aerodynamic forces such as buildings [11], bridges [12] and aircraft [13]. The flutter occurs due to the interaction between the aerodynamic forces, inertial forces and structure stiffness. The inertia due to aerodynamic forces and solid deformation normally increases as the flow speed increases and at a particular velocity the structure may lose stability and eventually fails. Loss of stability commonly occurs due to a monotonic divergence in deformation [14] or increased amplitude in structural oscillations known as flutter. Beyond the flutter speed, the amplitude of vibration becomes self-exciting. This self-excited amplitude along with the instability due to negative aeroelastic damping leads to rapid structural failure [6, 15, 16]. Many researchers have studied the flutter instability in different aeroelastic systems. A flexible mounting system was developed for flutter tests in the wind tunnel using rigid rings by De Marqui Junior et al. [17]. Their experimental system was used to investigate the onset of flutter while considering the combination of structural bending and torsion vibrational modes. In the same context, Hayat et al. [6] investigated the aeroelastic performance of a 5 MW wind turbine with shallow-angled skin of blades using the eigenvalue analysis. Asjes et al. [18] developed a modeling framework using a steady-state model for aerodynamic forces to predict the reliance of the flutter speed on various parameters of the model. Technically, when flexible airfoils experience excitation from the flow stream, flutter instability triggered by a Hopf bifurcation, may occur.

The capture of the critical nonlinear periodical behavior has been the focus of many researchers in aeroelasticity [19–22]. The sources of nonlinearity in aeroelastic systems include the structure, the material, the geometry, friction and flow separation [23, 24]. Lee et al. [25] presented a comprehensive study on these nonlinearities along with the derivation of the equations of motion of a 2D airfoil oscillating in pitch and plunge. In addition, the effect of nonlinear aeroelasticity and its association with limit cycle oscillations (LCO) was summarized by Dowell et al. [20]. The reader is also referred to [26, 27] for further understanding of the effect of structural nonlinearities on the dynamical behavior of aeroelastic systems. Strganac et al. [28] investigated the stability of a 2-DOF aeroelastic system by presenting a nonlinear partial feedback linearization controller. Ghommem et al. [3] used a quasi-steady aerodynamic model for a 2-DOF airfoil system to examine the impact of the uncertainty in the elastic properties on its nonlinear dynamic behavior.

The nonlinear response of aeroelastic systems can be captured and analyzed using numerical simulations obtained from the time integration of nonlinear equations of motion. The extensive required time for such simulations makes it unattractive from a practical viewpoint. As such, there is a need to develop reduced-order models to speed up the prediction the flutter and characterization of post-bifurcation behavior while maintaining good accuracy. To do so, several analytical approaches can be applied. For instance, the harmonic balance method (HBM) has been used in several work to predict the amplitude and frequency of limit cycle oscillations [20, 28–30]. The strength of the HBM lies in the computation of the transition curves between the stable and unstable dynamic solutions as demonstrated for 2D aeroelastic airfoil in [31]. The method of multiple scales (MMS), which is based on asymptotic perturbation, provides a more comprehensive analysis of nonlinear dynamic systems. MMS has been extensively used for the analysis of nonlinear systems including internal resonance problems [32], vortex-induced vibrations of rotating blades [33] and nonlinear interactions of bridge modes [34]. To examine the dynamic behavior of the Goland wing, Nayfeh et al. [35] applied MMS to derive its normal form. Likewise, Ghommem et al. [3] used the MMS

for the uncertainty analysis of a 2DOF aeroelastic system based on nonlinear quasi-steady aerodynamic model. Beran et al. [36] used an aerodynamic model derived from transonic small disturbance theory. They considered an aeroelastic system made of a wing and a store. Their model accounted for nonlinear structural, aerodynamic and store-induced effects. The placement of the store along the wing was found to have a significant impact in the nonlinear behavior and bifurcation characteristics of the coupled system. Theodorsen [37] developed an aerodynamic model valid only for the flight operation at small angles of attack which was widely used in the literature. Muturi et al. [38] conducted an experimental investigation of a pitch/plunge airfoil system with structural nonlinearity along the plunge direction. The combined aerodynamic and structural nonlinearities were observed to trigger LCOs whose amplitude remains steady over a range of flight speed if the aeroelastic system is initially excited above a critical value.

To overcome the undesirable vibrations resulting from the interactions of the aeroelastic system with the airstream, several vibration absorption techniques have been proposed [39, 39–43]. In highly flexible wing structures, piezoelectric materials are embedded to actuate wing warping which in turn control the vibration and/or morphs the wings. Tsushima and Su [39] investigated the impact of piezoelectric transduction on suppressing the passive flutter in highly flexible wings. Their study demonstrated the possible stabilization of the wing, while exploiting the energy of the flutter by properly placing the piezoelectric actuators and energy harvesters. In a recent paper, Kassem et al. [39] proposed a novel technique to suppress the flutter by using an active dynamic vibration absorber (ADVA). However, this flutter suppression technique requires auxiliary power source for operation. Verstraelen et al. [40] demonstrated experimentally the effectiveness of a single passive vibration absorber in delaying the flutter onset and the limit cycle oscillations. They conducted wind tunnel tests on a thin rectangular flat plate with an aspect ratio of 4. Their aeroelastic system was observed to undergo pitch and flap rotations. They reported a 30% increase in the flutter speed when deploying a single vibration absorber of around 2.3% of the total mass of the full system. The deployment of arrays of distributed tuned vibration absorbers (or referred to as tuned mass dampers) constitutes a versatile vibration control approach that has not been fully investigated for aircraft wings [41]. Yet, this vibration control strategy has been implemented on other types of aeroelastic systems including suspension bridges [42–44], wind turbines [45, 47], high-rise buildings [48] and rotating blades [49]. Casalotti et al. [42] conducted a numerical investigation to demonstrate the superior performance of hysteretic vibration absorbers over their linear counterparts to mitigate multi-mode flutter of long-span suspension bridges. Given their span length and cross-sectional aerodynamic shapes, such structures may experience two closely spaced flutter modes and then the use of linear mass dampers did not enable a significant shift in the flutter speed. The implementation of hysteretic vibration absorbers showed great capability to effectively control the induced vibrations in the post-flutter regime. The effectiveness of this type of vibration absorbers has been also studied for other engineering applications [49–54]. Basta et al. [48] investigated the nonlinear vibrations of a metamaterial rotating cantilever beam embedded with a periodic array of spring-mass-damper subsystems as vibration absorbers. The study demonstrated the ability of the local absorbers to efficiently suppress the amplitude of the oscillation of the system and further delay the critical speed at which the rotating beam starts to undergo in-plane vibrations. A design optimization under the influence of nonlinear tuned vibration absorbers for flutter control has been conducted by Malher et al. [55]. They showed the potential use of passive vibration absorber to significantly delay the flutter and avoid the subcritical instability.

The assessment of vibration control strategies requires a proper selection of the modes to capture the relevant and important dynamics of the aeroelastic systems and properly predict the flutter onset [35, 42, 56]. This is critical especially for long-span suspension bridges in which multi-mode flutter may occur and the loss of stability may occur through higher modes [42, 56]. Arena et al. [56] investigated the aerodynamic response of nanocomposite panels subject to supersonic flows. They used a nonlinear plate model combined with piston theory to analyze the flutter instability. A convergence analysis of the discretized form of continuous system revealed the need to select the first five modes to properly detect the flutter mode and its corresponding speed. In the present study, we consider a wing modeled as a 2DOF

system undergoing two coupled modes: pitching and plunging motions. Nayfeh et al. [35] developed reduced-order models of a Goland wing following two approaches: perturbation technique and discretization Galerkin procedure. They showed that use of the first bending and torsion modes in the discretized system leads to an accurate estimate of the flutter speed. The incorporation of higher modes improved the accuracy of the wing's response in the post-flutter regime.

In this work, we investigate flutter suppression using an array of distributed passive nonlinear vibration absorber. This falls under the category of metastructures. These structures are commonly conventional structures embedded with a lattice or a periodic geometry of small absorbers. This vibration control approach has not been fully explored for aircraft wings. The introduced model consists of a wing (modeled by a 2DOF system) integrated with an array of vibration absorbers. The entire system's mass is conserved which means that any added mass to the absorbers is taken from the mass of the host structure itself. The parameters of the aeroelastic metastructure are mainly the number of the vibration absorbers, their stiffness, damping coefficient and position from the elastic axis. It is shown in this study that a proper selection of these parameters is found to increase the flutter speed up to 84% compared to that reported previously when the aeroelastic system lacks vibration absorbers [3]. This enables extended range of safe flight operation. On the other hand, the structural nonlinearity of the vibration absorbers is observed ineffective in terms of reducing the amplitude of the limit cycle oscillation beyond flutter.

The remainder of the paper is organized as follows. In Sect. 2, the problem definition and derivation of governing equations of the system are introduced. This is followed by a parametric study of the linear parameters of the absorber(s) in Sect. 3. This includes the effect of placing an array of distributed absorbers on the flutter onset. Next, the MMS is applied to derive the normal form of the system to ease the computations and has a direct indication on the type of bifurcation. Consequently, the effect of the nonlinear parameters of the absorber is investigated. The effects of soft pitch springs and multiple absorbers on the post-flutter regime are also examined. Lastly, the main findings of the numerical study are summarized.

2 Mathematical Model of Conserved-mass Metamaterial Aeroelastic System

The conserved-mass aeroelastic metastructure system, considered in this work, is presented in Fig. 1. The airfoil is supported by nonlinear springs in the pitch, plunge and absorber directions. We attach to the aeroelastic system an array of distributed vibration absorbers. By a conserved system, it means that any increase in the mass of the absorbers comes at the expense of an equal cut from the host structure. In aerospace applications, it is crucial to maintain low levels of vibrations while deploying lightweight and robust materials. Preserving the total mass as this is important for aeroelastic systems as heavier structures may resist to incoming freestream, but this will be at the expense of fuel consumption. Each absorber i has its own mass, stiffness and damping. Moreover, it is free to be placed at a distance $l_i b$ from the elastic axis. As shown in Fig. 1, each passive vibration absorber comprises a cantilever beam with a tip mass, which is equivalent to a mass-spring-damper system. The wing is free to translate vertically (plunge) and rotate about the elastic axis (pitch).

Denoting by h, α and x_i the plunge deflection, pitch angle and i^{th} absorber deflection, respectively, one can write the governing equations of motion of the proposed aeroelastic airfoil system equipped with passive vibration absorbers (PVA) as

$$\begin{aligned} &m_T\ddot{h} + m_\alpha x_\alpha \ddot{\alpha} + c_h\dot{h} + \sum_{i=1}^{N_{ab}} c_{ab_i}\left(\dot{h} - \dot{x}_i - l_i b\dot{\alpha}\right) \\ &+ k_h h + \sum_{i=1}^{N_{ab}} k_{ab_i}(h - x_i - l_i b\alpha) = -L \\ &m_\alpha x_\alpha b\ddot{h} + I_\alpha\ddot{\alpha} + c_\alpha\dot{\alpha} + \sum_{i=1}^{N_{ab}} c_{ab_i} l_i b\left(\dot{x}_i - \dot{h} + l_i b\dot{\alpha}\right) \\ &+ k_\alpha\alpha + \sum_{i=1}^{N_{ab}} k_{ab_i} l_i b(x_i - h + l_i b\alpha) = M \end{aligned} \tag{1a}$$

And the equation of the ith absorber is

$$m_{ab_i}\ddot{x}_i + c_{ab_i}\left(\dot{x}_i - \dot{h} + l_i b\dot{\alpha}\right) + k_{ab_i}(x_i - h + l_i b\alpha) = 0 \tag{1b}$$

In matrix format, the equations of system can be written as follows:

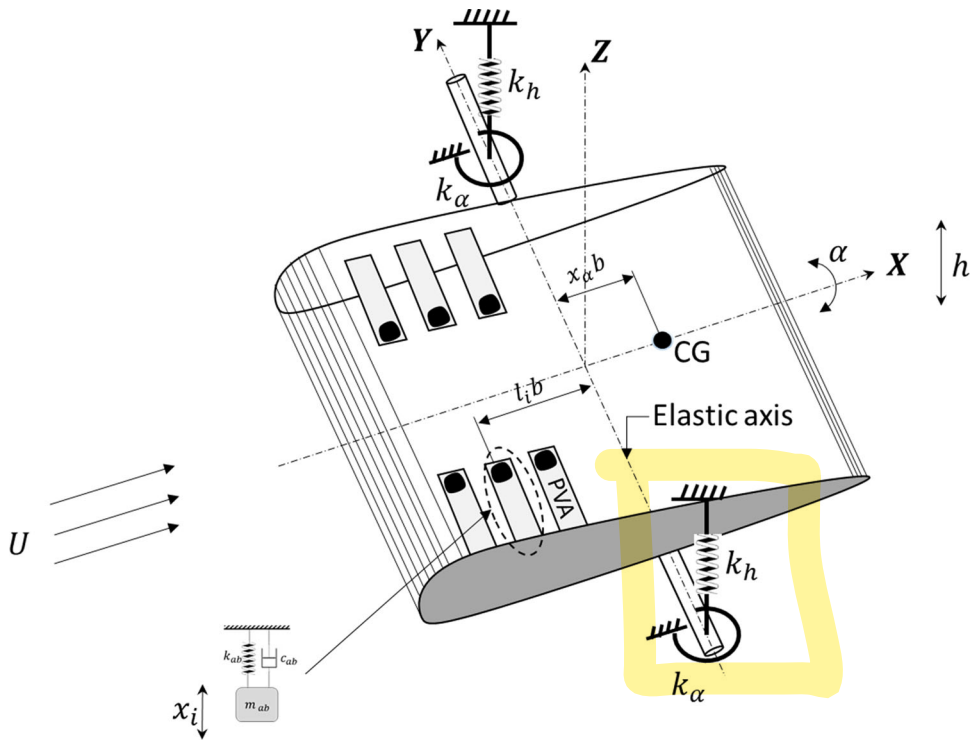

Fig. 1 Aircraft wing equipped with an array of passive vibration absorbers

$$\begin{pmatrix} m_T & m_\alpha x_\alpha & 0 & 0 & 0 \\ m_\alpha x_\alpha b & I_\alpha & 0 & 0 & 0 \\ 0 & 0 & m_{ab_i} & 0 & 0 \\ 0 & 0 & 0 & \ddots & 0 \\ 0 & 0 & 0 & 0 & m_{ab_{N_{ab}}} \end{pmatrix} \begin{pmatrix} \ddot{h} \\ \ddot{\alpha} \\ \ddot{x}_i \\ \vdots \\ x_{N_{ab}} \end{pmatrix} + \begin{pmatrix} c_h + \sum c_{ab_i} & \sum -c_{ab_i} l_i b & -c_{ab_i} & \cdots & -c_{ab_{N_{ab}}} \\ \sum -c_{ab_i} l_i b & c_\alpha + \sum c_{ab_i} l_i^2 b^2 & c_{ab_i} l_i b & \cdots & c_{ab_{N_{ab}}} l_{N_{ab}} b \\ -c_{ab_i} & c_{ab_i} l_i b & c_{ab_i} & 0 & 0 \\ \vdots & \vdots & 0 & \ddots & 0 \\ -c_{ab_{N_{ab}}} & c_{ab_{N_{ab}}} l_{N_{ab}} b & 0 & 0 & c_{ab_{N_{ab}}} \end{pmatrix} \begin{pmatrix} \dot{h} \\ \dot{\alpha} \\ \dot{x}_i \\ \vdots \\ \dot{x}_{N_{ab}} \end{pmatrix}$$
$$+ \begin{pmatrix} k_h + \sum k_{ab_i} & \sum -k_{ab_i} l_i b & -k_{ab_i} & \cdots & -k_{ab_{N_{ab}}} \\ \sum -k_{ab_i} l_i b & k_\alpha + \sum k_{ab_i} l_i^2 b^2 & k_{ab_i} l_i b & \cdots & k_{ab_{N_{ab}}} l_{N_{ab}} b \\ -k_{ab_i} & k_{ab_i} l_i b & k_{ab_i} & 0 & 0 \\ \vdots & \vdots & 0 & \ddots & 0 \\ -k_{ab_{N_{ab}}} & k_{ab_{N_{ab}}} l_{N_{ab}} b & 0 & 0 & k_{ab_{N_{ab}}} \end{pmatrix} \begin{pmatrix} h \\ \alpha \\ x_i \\ \vdots \\ x_{N_{ab}} \end{pmatrix} = \begin{pmatrix} -L \\ M \\ 0 \\ \vdots \\ 0 \end{pmatrix} \tag{2}$$

where m_T is the total mass of the wing and its support structure; m_α is the wing mass alone; m_{ab_i} is the mass of the ith absorber. N_{ab} is the total number of absorbers. Note that the total mass is conserved. In other words, the additional mass to the system coming from the total absorbers $\sum_{i=1}^{N_{ab}} m_{ab_i}$ is taken from the main structure's mass m_T to keep the total mass of the aeroelastic system constant. The conserved-mass approach was used to ensure that the vibration

mitigation occurs due to the metastructure and not because of mass added to the system. I_α is the mass moment inertia about the elastic axis; b is the half chord length; x_α is the nondimensional distance between the center of mass and the elastic axis; l is the nondimensional distance between the elastic axis and the position of the PVA. A linear viscous damping model is considered. c_h and c_α are the plunge and pitch viscous damping coefficients, respectively, while c_{ab_i} denotes the ith absorber damping coefficient; L and M denote the lift and the aerodynamic moment about the elastic axis, respectively. k_h, k_α and k_{ab_i} are the structural stiffness for the plunge, pitch and ith absorber motions, respectively. The representative parameters of these stiffnesses are approximated in a polynomial form as

$$\begin{aligned} k_h(h) &= k_{h0} + k_{h1}h + k_{h2}h^2 + \ldots \\ k_\alpha(\alpha) &= k_{\alpha 0} + k_{\alpha 1}\alpha + k_{\alpha 2}\alpha^2 + \ldots \\ k_{ab}(x) &= k_{ab0} + k_{ab1}x + k_{ab2}x^2 + \ldots \end{aligned} \tag{3}$$

The nonlinear stiffness coefficients reported in Eq. (3) are obtained from the experimental study (wind tunnel investigations) conducted by Strganac et al. [57] who performed parameter identification to come up with the nonlinear representation of the springs to model the stiffness along the plunge and pitch modes.

There are many possible aerodynamic models available in the literature to represent the unsteady lift and moment loads. In this study, we adopt the aerodynamic model used by Strganac et al. [57] which was proven appropriate for the low, reduced frequency, subsonic flow as demonstrated through the experiments reported in [57]. In this model, the aerodynamic loads are evaluated using a quasi-steady approximation with a stall model and written as [28, 44]

$$\begin{aligned} L &= \rho U^2 b c_{l_\alpha}\left(\alpha_{eff} - c_s\alpha_{eff}^3\right) \\ M &= \rho U^2 b^2 c_{m_\alpha}\left(\alpha_{eff} - c_s\alpha_{eff}^3\right) \end{aligned} \tag{4}$$

where U is the freestream velocity, c_{l_α} and c_{m_α} are the aerodynamic lift and moment coefficients, and c_s is a nonlinear parameter associated with stall. The effective angle of attack due to the instantaneous motion of the airfoil is given by [28]

$$\alpha_{eff} = \left[\alpha + \frac{\dot{h}}{U} + \left(\frac{1}{2} - a\right)b\frac{\dot{\alpha}}{U}\right] \tag{5}$$

where a is the nondimensional distance from the midchord to the elastic axis.

The theoretical investigation is performed first on a single vibration absorber. Therefore, the subsequent modeling equations are presented for a single absorber. Without loss of generality, these can be extended to multiple absorbers. For the sake of subsequent analyses, the state variables are defined as

$$\boldsymbol{Y} = \begin{pmatrix} Y_1 \\ Y_2 \\ Y_3 \\ Y_4 \\ Y_5 \\ Y_6 \end{pmatrix} = \begin{pmatrix} h \\ \alpha \\ x \\ \dot{h} \\ \dot{\alpha} \\ \dot{x} \end{pmatrix} \tag{6}$$

and the equations of motion are written in the form

$$\dot{\boldsymbol{Y}} = F(\boldsymbol{Y}, U) \tag{7}$$

where

$$F(\boldsymbol{Y}, U) = \begin{pmatrix} Y_4 \\ Y_5 \\ Y_6 \\ -p_h(\boldsymbol{Y}_1, \boldsymbol{Y}_3)Y_1 - (k_1U^2 + p_\alpha(\boldsymbol{Y}_2, \boldsymbol{Y}_3))Y_2 + S_{1d}(\boldsymbol{Y}_3)Y_3 - c_1Y_4 - c_2Y_5 + c_5Y_6 + g_{NL1} \\ -q_h(\boldsymbol{Y}_1, \boldsymbol{Y}_3)Y_1 - \left(k_2U^2 + q_\alpha(\boldsymbol{Y}_2, \boldsymbol{Y}_3)\right)Y_2 - S_{2d}(\boldsymbol{Y}_3)Y_3 - c_3Y_4 - c_4Y_5 - c_6Y_6 + g_{NL2} \\ o_1(\boldsymbol{Y}_3)Y_1 - o_2(\boldsymbol{Y}_3)Y_2 - o_1(\boldsymbol{Y}_3)Y_3 + o_3Y_4 - o_4Y_5 - o_3Y_6 \end{pmatrix} \tag{8}$$

The relations of the variables used in Eq. (8) to the physical parameters are provided in Table 1. These parameters are obtained after converting the equations of motion in the state space form. This form is required for the numerical implementation of the equations and the derivation of the normal form using the method of multiple scales. The original governing equations, Eq. (7) can be written in compact form as

$$\dot{\boldsymbol{Y}} = A(U)\boldsymbol{Y} + NL\left(\boldsymbol{Y}^2, \boldsymbol{Y}^3\right) \tag{9}$$

where

$$A(U) = \begin{pmatrix} 0 & 0 & 0 & 1 & 0 & 0 \\ 0 & 0 & 0 & 0 & 1 & 0 \\ 0 & 0 & 0 & 0 & 0 & 1 \\ -\dfrac{[I_\alpha k_{h_0} + k_{d_0}(I_\alpha + lb^2 m_w x_\alpha)]}{d} & -\left(k_1 U^2 + \dfrac{[-m_w x_\alpha b k_{\alpha_0} - k_{d0} lb(I_\alpha + lb^2 m_W x_\alpha)]}{d}\right) & \dfrac{[k_{d0}(I_\alpha + m_w x_\alpha lb^2)]}{d} & -c_1 & -c_2 & -c_5 \\ -\dfrac{[-m_w x_\alpha b k_{h_0} - k_{d0} b(lm_T + m_w x_\alpha)]}{d} & -\left(k_2 U^2 + \dfrac{[\boldsymbol{m_T} k_{\alpha 0} + k_{d0}\boldsymbol{lb^2}(\boldsymbol{m_T l} + \boldsymbol{m_w x_\alpha})]}{\boldsymbol{d}}\right) & -\dfrac{[k_{d0} b(lm_T + m_w x_\alpha)]}{d} & -c_3 & -o_4 & -o_3 \\ \dfrac{k_{d0}}{m_d} & -\dfrac{[blk_{d_0}]}{m_d} & -\dfrac{k_{d0}}{m_d} & -o_3 & -c_1 & -c_1 \end{pmatrix} \tag{10}$$

and

$$NL(\boldsymbol{Y}^2, \boldsymbol{Y}^3) = \begin{pmatrix} 0 \\ 0 \\ 0 \\ -\left(\dfrac{[(k_{d_1}\boldsymbol{Y}_3 + k_{d_2}\boldsymbol{Y}_3^2)(I_\alpha + lb^2 m_w x_\alpha)]}{d}\right)\boldsymbol{Y}_1 - \left(\dfrac{[-m_w x_\alpha b(k_{\alpha_1}\boldsymbol{Y}_2 + k_{\alpha_2}\boldsymbol{Y}_3^2) - (k_{d_1}Y_3 + k_{d_2}\boldsymbol{Y}_3^2) lb(I_\alpha + lb^2 m_W x_\alpha)]}{d}\right)\boldsymbol{Y}_2 + \left(\dfrac{[(k_{d_1}\boldsymbol{Y}_3 + k_{d_2}\boldsymbol{Y}_3^2)(I_\alpha + m_w x_\alpha lb^2)]}{d}\right)\boldsymbol{Y}_3 \\ -\left(\dfrac{[-(k_{d_1}\boldsymbol{Y}_3 + k_{d_2}\boldsymbol{Y}_3^2) b(lm_T + m_w x_\alpha)]}{d}\right)\boldsymbol{Y}_1 - \left(\dfrac{[m_T(k_{\alpha_1}\boldsymbol{Y}_2 + k_{\alpha_2}\boldsymbol{Y}_2^2) + (k_{d_1}Y_3 + k_{d_2}\boldsymbol{Y}_3^2) lb^2(m_T l + m_w x_\alpha)]}{d}\right)\boldsymbol{Y}_2 - \left(\dfrac{[(k_{d_1}\boldsymbol{Y}_3 + k_{d_2}\boldsymbol{Y}_3^2) b(lm_T + m_w x_\alpha)]}{d}\right)\boldsymbol{Y}_3 \\ \left(\dfrac{(k_{d_1}\boldsymbol{Y}_3 + k_{d_2}\boldsymbol{Y}_3^2)}{m_d}\right)\boldsymbol{Y}_1 - \left(\dfrac{[bl(k_{d_1}\boldsymbol{Y}_3 + k_{d_2}\boldsymbol{Y}_3^2)]}{m_d}\right)\boldsymbol{Y}_2 - \left(\dfrac{(k_{d_1}\boldsymbol{Y}_3 + k_{d_2}\boldsymbol{Y}_3^2)}{m_d}\right)\boldsymbol{Y}_3 \end{pmatrix} \tag{11}$$

The preceding matrices in Eqs. (10) and (11) will be then used separately in the subsequent sections. The system's stability, for instance, is determined by considering the linearized governing equations which is grouped in $A(U)$. On the other hand, the nonlinear aspects of the response are investigated by the normal form where the full nonlinear set of equations are included. This is also verified by the numerical integration where the system's nonlinearities are included.

The present model is used to conduct a parametric study with a goal to gain insights on the effectiveness of the conserved-mass metastructure concept (array of distributed tuned mass dampers) for the design enhancement of aircraft wings and provide guidance for the appropriate selection of the absorbers' characteristics to achieve further resistance to the induced vibrations due to air-structure interactions as will be shown in the subsequent section.

3 Results and discussion

In this section, we conduct linear and nonlinear analyses to determine the impact of the array of passive vibration absorbers on the dynamic response of the aeroelastic system. In particular, we investigate its effect on delaying the flutter onset and reducing the

Table 1 Aeroelastic system parameters

$$
\begin{aligned}
d &= m_T I_\alpha - m_w^2 x_\alpha^2 b \\
k_1 &= \left(I_\alpha \rho b C_{l_\alpha} + m_w x_\alpha \rho b^3 c_{m_\alpha}\right)/d \\
k_2 &= -\left(m_w x_\alpha \rho b^2 c_{l_\alpha} + m_T \rho b^2 c_{m_\alpha}\right)/d \\
c_1 &= \left[I_\alpha (c_h + \rho_U b C_{l_\alpha}) + m_w x_\alpha \rho U b^3 c_{m_\alpha} + c_d \left(I_\alpha + m_w x_\alpha l b^2\right)\right]/d \\
c_2 &= \left[I_\alpha \rho U b^2 C_{l_\alpha} \left(\tfrac{1}{2} - a\right) - m_w x_\alpha b c_\alpha - c_d l b \left(I_\alpha + l b^2 m_w x_\alpha\right) + m_w x_\alpha \rho U b^4 c_{m_\alpha} \left(\tfrac{1}{2} - a\right)\right]/d \\
c_3 &= \left[-m_w x_\alpha b \left(c_h + \rho U b C_{l_\alpha}\right) - m_T \rho U b^2 c_{m_\alpha} - c_d b (l m_T + m_w x_\alpha)\right]/d \\
c_4 &= \left[m_T \left(c_\alpha - \rho U b^3 c_{m_\alpha} \left(\tfrac{1}{2} - a\right)\right) - m_w x_\alpha \rho U b^3 c_{l_\alpha} \left(\tfrac{1}{2} - a\right) + c_d l b^2 (l m_T + m_w x_\alpha)\right]/d \\
c_5 &= \left[c_d \left(I_\alpha + l b^2 m_w x_\alpha\right)\right]/d \\
c_6 &= \left[c_d b (l m_T + m_w x_\alpha)\right]/d \\
p_\alpha(Y_2, Y_3) &= \left[-m_w x_\alpha b k_\alpha(Y_2) - k_d(Y_3) l b \left(I_\alpha + l b^2 m_W x_\alpha\right)\right]/d \\
q_\alpha(Y_2, Y_3) &= \left[m_T k_\alpha(Y_2) + k_d(Y_3) l b^2 (m_T l + m_w x_\alpha)\right]/d \\
p_h(Y_1, Y_3) &= \left[I_\alpha k_h(Y_1) + k_d(Y_3) \left(I_\alpha + l b^2 m_w x_\alpha\right)\right]/d \\
q_h(Y_1, Y_3) &= \left[-m_w x_\alpha b k_h(Y_1) - k_d(Y_3) b (l m_T + m_w x_\alpha)\right]/d \\
s_{1_d}(Y_3) &= \left[k_d(Y_3) \left(I_\alpha + m_w x_\alpha l b^2\right)\right]/d \\
s_{2_d}(Y_3) &= \left[k_d(Y_3) b (l m_T + m_w x_\alpha)\right]/d \\
g_{NL1} &= \left(c_s \rho U^2 b\right) \left(c_{l_\alpha} I_\alpha + m_w x_\alpha b^2 c_{m_\alpha}\right) \alpha_{Eff}^3/d \\
g_{NL2} &= -\left(c_s \rho U^2 b^2\right) \left(c_{l_\alpha} m_w x_\alpha + m_T c_{m_\alpha}\right) \alpha_{eff}^3/d \\
O_1(Y_3) &= k_d(Y_3)/m_d \\
O_2(Y_3) &= [b l k_d(Y_3)]/m_d \\
O_3 &= c_d/m_d \\
O_4 &= [b l c_d]/m_d
\end{aligned}
$$

limit cycle oscillations near the Hopf bifurcation. The absorber's stiffness is denoted in Eq. (3) as k_{ab}. To put this value into perspective, it is perceived better to relate directly to the natural frequency associated with the plunging motion of the aeroelastic system. As such, we introduce the frequency ratio η expressed as

$$\eta = \frac{\omega_{ab}}{\omega_h} = \frac{\sqrt{\frac{k_{ab0}}{m_{ab}}}\sqrt{1 - \zeta_{ab}^2}}{\sqrt{\frac{k_{h0}}{m_T}}\sqrt{1 - \zeta_h^2}} \tag{12}$$

where the damping ratio is given by $\zeta = \frac{c}{2\sqrt{km}}$. This frequency ratio between the damped natural frequencies of the absorber and the plunging motion will be used in the interpretation of the subsequent numerical results.

Table 2 Passive vibration absorber parameters

k_{ab}(N/m)	c_{ab}(Kg/s)	m_{ab}	l
2000	0.001	$1\% of m_T$	1.25

3.1 Stability analysis and flutter speed

We first conduct a linear analysis of the aeroelastic system based on a single vibration absorber. Then, we extend our analysis to an array of distributed vibration absorbers and investigate their impact on the flutter onset. We determine the stability of the system by computing the eigenvalues of the matrix $A(U)$. The linear analysis enables to determine the impact of incorporating a passive vibration absorber on the flutter speed. Moreover, we investigate the effect of the stiffness and damping characteristics of the absorber on the occurrence of flutter. The 6 by 6 matrix $A(U)$ given in Eq. (11) has a set of six complex-conjugate eigenvalues, denoted by $\{\rho_j, j = 1, 2, ..., 6\}$. We note that this matrix is a function of the air speed U. These eigenvalues determine the stability of the trivial solution of the linear part of Eq. (9). If the real parts of all of the ρ_j are negative, the trivial solution is asymptotically stable. On the other hand, if the real part of one or more eigenvalues are positive, the trivial solution is

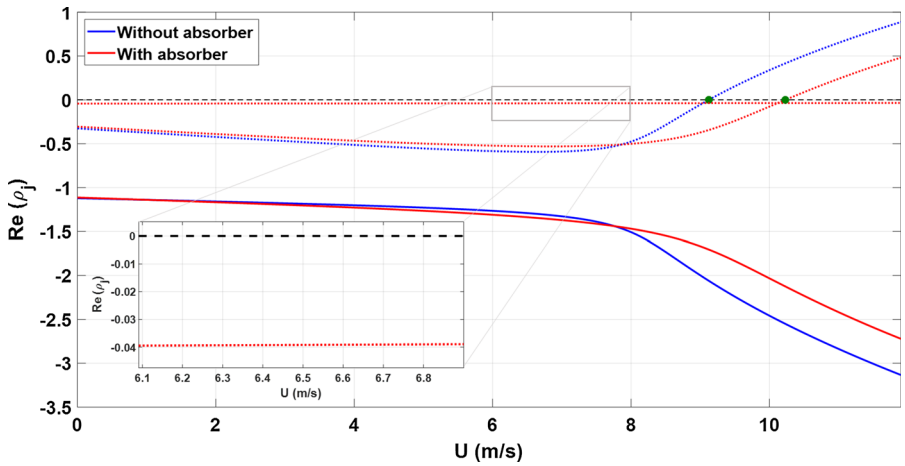

(a) Real part of the eigenvalues (decay/growth rate)

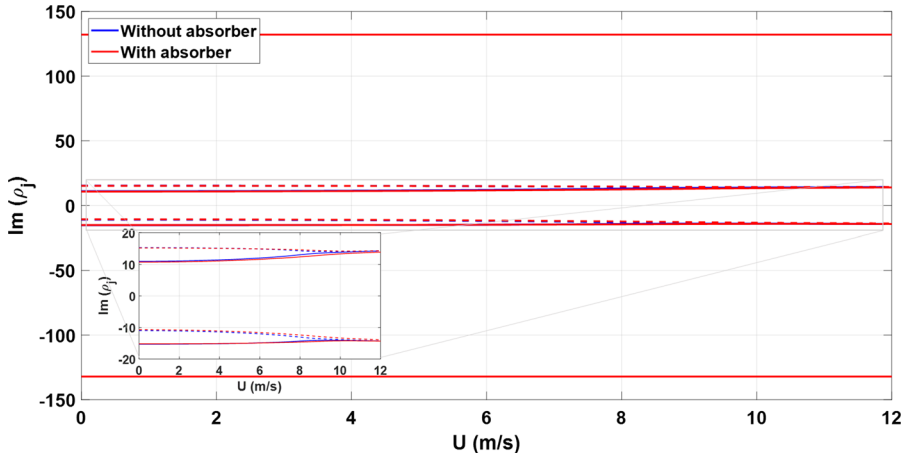

(b) Imaginary part of the eigenvalues (frequency)

Fig. 2 Variations of the **a** real and **b** imaginary parts of the eigenvalues with the freestream velocity U

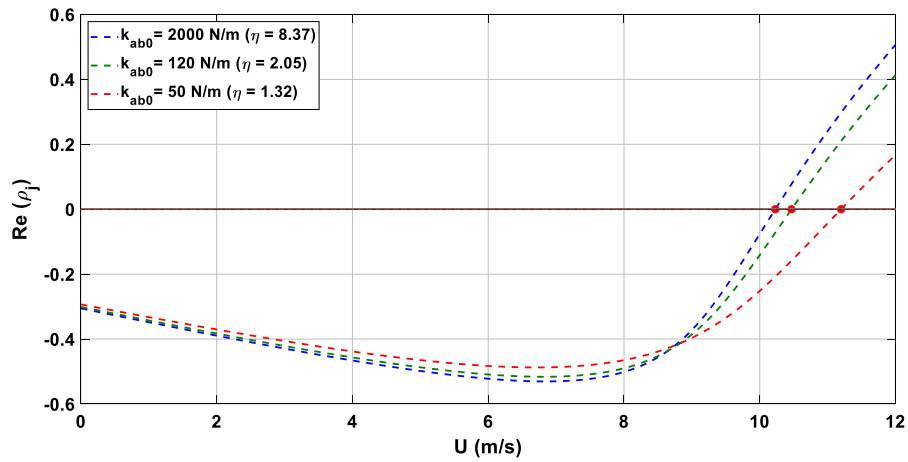

Fig. 3 Variations of the real parts of the eigenvalues with the freestream velocity U for different stiffness of the vibration absorber

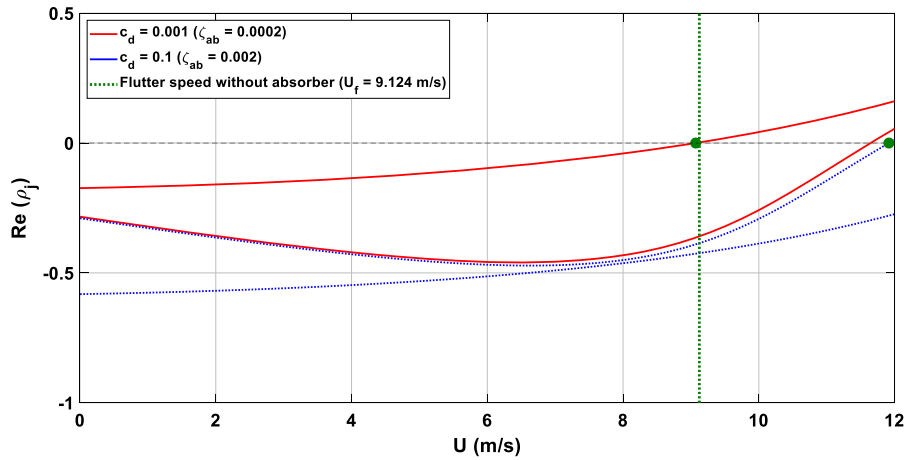

Fig. 4 Effect of the damping coefficient of the absorber on the flutter speed

unstable. The flutter speed, denoted by U_f, at which a pair of complex-conjugate eigenvalues have zero real parts, corresponds to the onset of linear instability. For the specific values given in [28] and Table 2 for the passive vibration absorber parameters, Fig. 2a and b shows the variation of the real and imaginary parts of the eigenvalues of the matrix $A(U)$ with the air speed U, respectively.

As mentioned, flutter speed occurs when the real part of some of the eigenvalues of the matrix $A(U)$ shifts from negative to positive values. As shown in Fig. 2a, the flutter speed is delayed from $U_f = 9.124\,\mathrm{m/s}$ to $U_f = 10.229\,\mathrm{m/s}$. We note that the flutter speed corresponding to the system without absorber was reported in [3]. The results demonstrate that more than 9% increase in the flutter speed when equipping the aeroelastic system with a passive vibration absorber is achieved, as per the specifications shown in Table 2. Figure 2a and b shows three pairs of complex-conjugate eigenvalues. The new pair of the eigenvalues is associated with the vibration absorber that corresponds to a stable solution as indicated by the positive values of their real parts. As seen in the zoomed window, the solution does not cross the x-axis and remains negative for the entire range of the air speed. Inspecting Fig. 2b, we observe that imaginary parts (frequencies) associated with the plunging and pitching motions merge at $U_f = 10.3\,\mathrm{m/s}$ for the case with absorber. At this speed, the aeroelastic system undergoes a Hopf bifurcation.

Next, we fix the position of the absorber by keeping the parameter l constant and equal to 1.25 while varying its stiffness and damping coefficients. The objective is to examine their combined effect on the flutter speed. The effect of the linear stiffness coefficient of the absorber on the flutter speed is illustrated in Fig. 3. Clearly, the stiffness of the absorber, denoted by k_{ab0}, affects the flutter speed as indicated

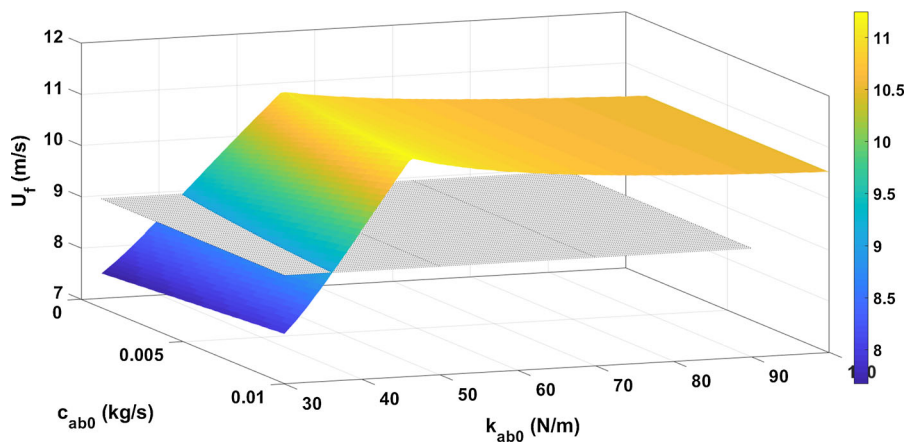

Fig. 5 3D plot of flutter speed vs. the stiffness and damping coefficient of the absorber

by the crossing of the real part of the eigenvalues the x-axis at different speeds. Note that there are more real parts of the eigenvalue like the previous figures, but only the real part of the eigenvalues which cross the x-axis is presented for clarity. For all cases, the damping coefficient c_{ab} is kept equal to 0.01 Kg/s. By keeping all other parameters constant, a decrease in the linear stiffness coefficient results in a further delay of the flutter speed and ranges from $U_f = 10.2290\,\mathrm{m/s}$ to $U_f = 11.119\,\mathrm{m/s}$. The latter flutter speed occurs at a linear stiffness of $k_{ab0} = 50N/m$ which corresponds to a frequency ratio $\eta = 1.32$; that is, the natural frequency of the absorber is 32% higher than that associated with the plunging motion. This constitutes a significant improvement in terms of flutter occurrence in comparison with the original aeroelastic system without absorber presented in [3] who reported a flutter speed of 9.1242 m/s (about 22% increase in the flutter speed). We expand our numerical study by investigating the effect of the damping coefficient of the absorber, as will be presented next.

Figure 4 shows the effect of the damping coefficient while keeping the linear stiffness coefficient of the absorber equal to $k_{ab0} = 40\mathrm{N/m}$. In this outcome, k_{ab0} is chosen to be $40N/m$ because the impact of the damping is more noticeable. Moreover, it is worth to showcase a scenario where adding an absorber of this stiffness can degrade the performance. This will be elaborated momentarily. Just like the previous figure, only the real part of the eigenvalues which cross the x-axis is presented. The increase in the damping coefficient results in a significant increase in the flutter speed. In particular, the value of the flutter speed is observed to increase from $9.07\,\mathrm{m/s}$ to $11.98\,\mathrm{m/s}$ when setting the damping ratio equal to $\zeta_{ab} = 0.02$. We note that this comparison is made with respect to the first configuration, where $c_{ab} = 0.001$ Kg/s ($\zeta_{ab} = 0.002$) and $k_{ab0} = 40\mathrm{N/m}$. For this case, despite the deployment of the absorber, the flutter speed was found equal to $U_f = 9.07\,\mathrm{m/s}$ which is actually worse than the system without absorber reported in [3]. The dashed vertical line in Fig. 4 indicates the flutter speed of the system without absorber. These results reveal that merely adding an absorber to the system does not guarantee an improvement in the performance of the system in terms of resistance to incoming airstream. In fact, it is shown that a particular combination of the vibration absorber can result in a worse flutter. As such, it is worth to see the combined effect of the stiffness and damping coefficients on the flutter occurrence.

The 3D plot showing the variations of the flutter speed of the aeroelastic system with the stiffness and damping coefficients is displayed in Fig. 5. The light shaded plane corresponds to $U_f = 9.124\,\mathrm{m/s}$ which is the flutter speed of the system without absorber [3].

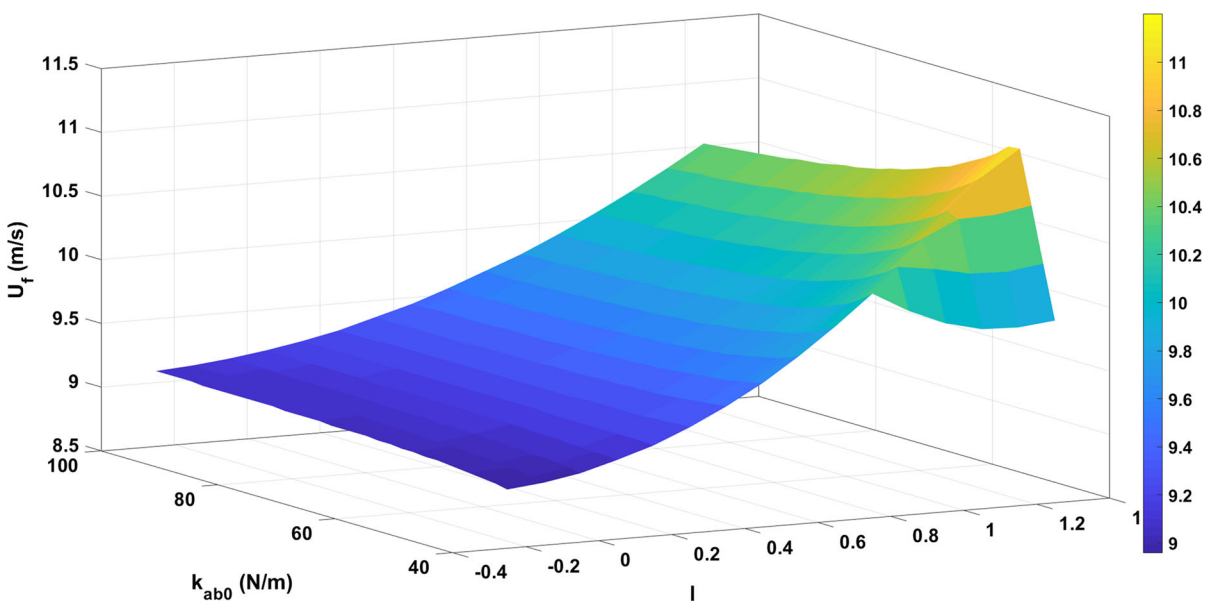

Fig. 6: 3D plot of flutter speed vs the stiffness and position of the absorber

The 3D plot enables to visualize the combined effect of the stiffness and damping of the absorber on the flutter onset. The frequency ratio ranges from $\eta = 1.0246$ to $\eta = 1.8707$. Of interest, the vibration absorber is observed to degrade the performance of the aeroelastic system when setting its linear stiffness coefficient equal or less than 40N/m, regardless of the value of its associated damping. On the other hand, a significant improvement can be achieved with the proper selection of k_{ab0} and c_{ab}. Indeed, the flutter speed is observed to reach more than 11 m/s when setting k_{ab0} equal to 46.5 N/m ($\eta = 1.2756$) and the damping coefficient c_{ab} equal to 0.01 kg/s. Beyond this point, increasing the stiffness of the absorber does not lead to any further increase in the flutter speed. However, the saturated flutter speed is relatively higher than the flutter speed without absorber. Conversely, below 40 N/m, there is a degradation in the flutter speed when compared to the system without absorber. This demonstrates the need for the proper selection of the vibration absorber characteristics to suppress flutter. Moreover, it is noticed that altering the stiffness of the absorber has a greater impact on the flutter speed of the system than that of the damping coefficient.

Another important system's parameter that can be controlled to maximize the vibration suppression is the position of the absorber with respect to the elastic axis. In Fig. 6, we show the combined effect of the stiffness and the position of the absorber on the flutter speed. The figure shows that when setting the linear stiffness coefficient of the vibration absorber equal to $k_{ab0} = 40\text{N/m}$, the aeroelastic system shows its best performance (i.e., maximum flutter speed) at $l = 0.8$. We recall that l represents the dimensionless distance (with respect to the wing's span) between the vibration absorber and the elastic axis. Positive and negative values of the parameter l indicate the placement of the vibration absorber ahead and behind the elastic axis, respectively. Figure 6 reveals that placing the absorber closer to the leading edge results in an increase in the flutter speed. The positions start from $l = -0.25$ to $l = 1.25$ with an increment of 0.25. This means that the absorber is initially placed behind the elastic axis and moved all the way close to the leading edge. The results show that the flutter speed is greatly affected by the position of the vibration absorber. Placing it further ahead the elastic center results in an increase in the flutter speed. Both the distance and position of the vibration absorber with respect to the elastic axis of the aeroelastic system have an impact on the onset of flutter. For example, the flutter speed at $l = -0.2$ is observed to be always worse than its counterpart at $l = 0.2$. These results demonstrate the importance of the proposer placement of the absorber to maximize its efficiency in terms of delaying the flutter.

The linear analysis shows that the position of the vibration absorber can greatly impact the performance of the system. By placing a vibration absorber with a linear stiffness of $k_{ab0} = 46.5\text{N/m}$ ($\eta = 1.2756$) at a distance of 1.25 in front of the elastic axis, the flutter speed experiences a 23.4% increase. The previous numerical study showed in detail the effect of a single vibration absorber on the aeroelastic behavior. The impact of embedding multiple absorbers (a metastructure) is investigated next.

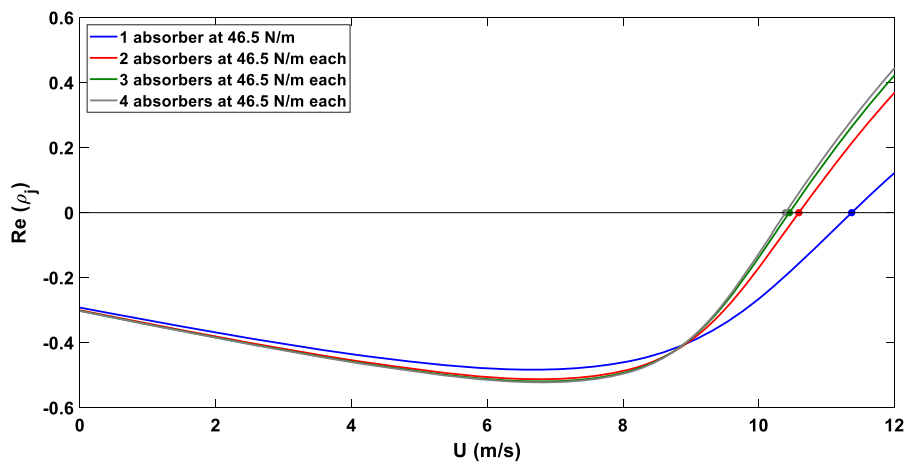

Fig. 7 Variations of the real parts of the eigenvalues with the freestream velocity U for varying number of absorbers and constant absorber(s) stiffness

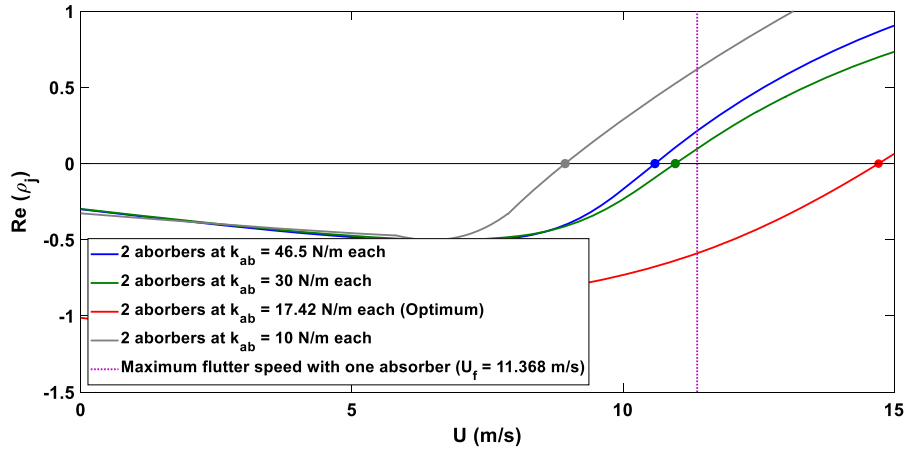

Fig. 8 Variations of the real parts of the eigenvalues with the freestream velocity U for two absorbers at different stiffnesses

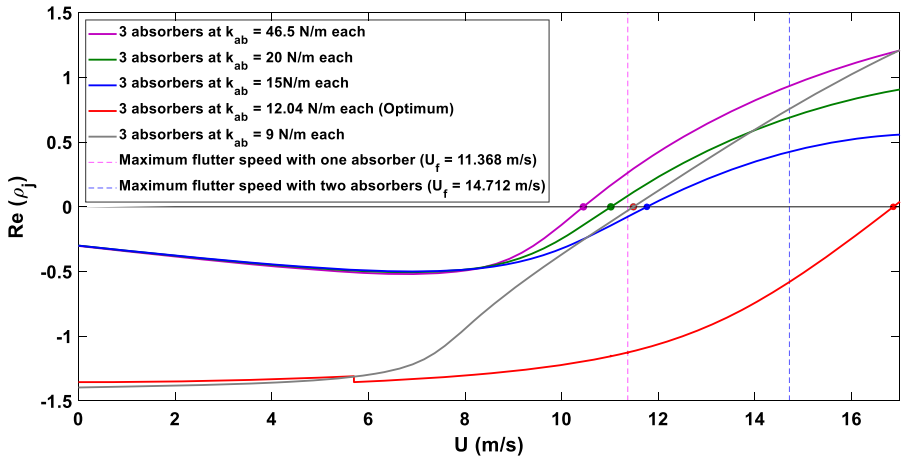

Fig. 9 Variations of the real parts of the eigenvalues with the freestream velocity U for three absorbers at different stiffnesses

3.2 Metastructure analysis

In this section, the effect of assembling a metastructure on the flutter speed is investigated. Here, the metastructure is the airfoil embedded with a varying number of vibration absorbers. Most importantly in our case, the mass of the metastructure is conserved regardless the number of these absorbers. A ratio of 1% taken of the host structure is kept constant for all cases. This means that 1% of the airfoil is devoted for the mass of the absorber(s). The mass ratio is divided equally among the absorber(s), but the entire mass of the system remains the same. Moreover, from the analysis presented previously, the absorbers are placed closer to the leading edge. In the preceding section, it is shown that a linear stiffness of $k_{ab0} = 46.5N/m$ at a distance of 1.25 ahead of the elastic axis gave the optimal conditions for the furthest delay in the flutter onset for a single absorber. To begin with the analysis of a general metastructure, a case study is considered to gain insight on the impact of the number of vibration absorbers on the flutter speed. The number of absorbers is varied from one to four, and the same optimal conditions obtained for the single resonator condition are applied to all cases. The corresponding simulation results are shown in Fig. 7. The results are presented in terms of the variations of the eigenvalues with the air speed. We observe that using the same stiffness, a single absorber outperforms the arrays of varying number of the absorbers. This observation is anticipated since a single absorber usually has higher impact as the 1% mass devoted to the damping is lumped in one single absorber. In fact, the use of a single resonator may lead to an optimum control at a

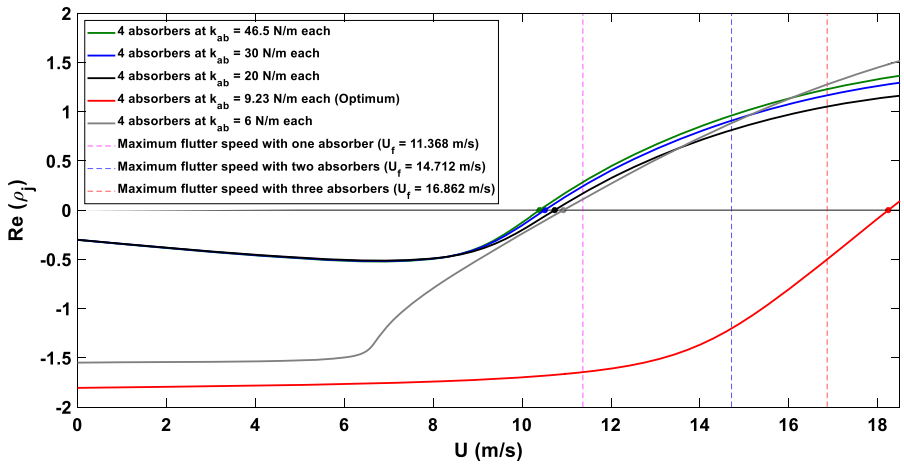

Fig. 10 Variations of the real parts of the eigenvalues with the freestream velocity U for four absorbers at different stiffnesses

Table 3 Summary of absorbers/stiffness/location combinations and their corresponding flutter speed

Number of absorbers	Stiffness (Each)	Location	Flutter Speed (U_f)
1	46.5	1.25	11.3680
2	46.5	1.24,1.26	10.5807
2	46.5	1.25,1.26	10.5890
2	30	1.25,1.26	10.953
2	17.42	1.25,1.26	14.712
2	10	1.25,1.26	8.93259
3	46.5	1.25,1.26,1.27	10.449
3	30	1.25,1.26,1.27	10.6280
3	20	1.25,1.26,1.27	11.0170
3	12.04	1.25,1.26,1.27	16.862
3	10	1.25,1.26,1.27	13.0744
4	46.5	1.25,1.26,1.27,1.28	10.394
4	30	1.25,1.26,1.27,1.28	10.51
4	20	1.25,1.26,1.27,1.28	10.733
4	9.23	1.25,1.26,1.27,1.28	18.238
4	6	1.25,1.26,1.27,1.28	10.9290

given absorber stiffness. However, it suffers from practical limitations and drawbacks due to mass concentration. The single absorber creates a concentrated point force acting on the beam. This attached mass can lead to high stress concentration in the region of contact. Therefore, the use of distributed absorbers is preferable. Moreover, in our study, another important advantage shows up when we further investigate the impact of progressively increasing the number of absorbers on the aeroelastic behavior.

Figure 8 displays the simulation results obtained for different cases when embedding two vibration absorbers while varying their stiffness. Considering more than one absorber with lower stiffness is observed to increase the flutter speed. Figure 5 shows that for a single absorber, a stiffness below than $k_{ab0} = 40$ N/m deteriorates the performance of the system. On the other hand, Fig. 8 reveals the possibility to delay the flutter onset when using two vibration absorbers with lower stiffness. Similar to the single absorber, the case with two absorbers has an optimal stiffness value which is found around 17.42 N/m for each absorber. The condition with two optimized absorbers leads to a significant increase in the flutter

speed in comparison with the one achieved using one single absorber. The latter is denoted by the vertical pink dashed line in Fig. 8. This constitutes another advantage of placing multiple absorbers along the wing. This phenomenon is further investigated when considering three vibration absorbers. The corresponding simulation results obtained for varying stiffness are shown in Fig. 9. Of interest, the flutter onset is delayed further compared to a single and double resonator. The optimum conditions for the single and double absorbers are shown in pink and blue vertical dashed lines, respectively. Setting the stiffness value to 12.04N/m for each vibration absorber gives the most optimal results when three absorbers are embedded to the aeroelastic system. This reveals the benefit of placing several vibration absorbers with lower stiffness values rather than using a single absorber. The optimal condition for three absorber gives a delayed flutter occurring at the speed of $U_f = 16.862\,\mathrm{m/s}$. Finally, the case with four absorbers is presented in Fig. 10. A similar trend is obtained. Indeed, the advantage of using a larger number of vibration absorbers while reducing their stiffness is confirmed. For the case of four absorbers, the optimal stiffness of each vibration absorber is found equal to 9.23 N/m which results in a larger flutter speed of 18.234 m/s. This constitutes an increase of 84% in the flutter speed in comparison with the aeroelastic system without absorbers and around 48.3% in comparison with the one equipped with one single absorber. This is attractive since a great delay in the flutter onset can be attained by distributing more vibration absorbers along the wing while setting their stiffness at lower values.

To gain further insight on the design of the conserved-mass metastructure aeroelastic system, a summary of the impact of the number of the vibration absorbers, their stiffness and their placement on the flutter speed is presented in Table 3. The simulation results reveal that a proper selection of the aforementioned parameters results in a significant increase in the flutter speed while preserving the total mass of the aeroelastic system. This shows the potential use of metastructures to achieve extended safe flight operation of aeroelastic systems.

Next, we incorporate the aeroelastic system's nonlinearities and examine the nonlinear dynamic response beyond the flutter (Hopf bifurcation).

3.3 Nonlinear reduced-order model

In this section, we use the method of multiple scales to develop the normal form of the aeroelastic system that constitutes the reduced-order analytical model. This will be verified against numerical integration of the governing equations. We derive the normal form that enables the representation of the aeroelastic system in the vicinity of the Hopf bifurcation that takes place at the flutter (i.e., $U = U_f$). To do so, we follow Nayfeh and Balachandran [58] and introduce a small bookkeeping parameter ε and seek a third-order approximate solution of Eq. (9) in the form

$$\boldsymbol{Y}(t) = \varepsilon \boldsymbol{Y}_1(T_0, T_2) + \varepsilon^2 \boldsymbol{Y}_2(T_0, T_2) + \varepsilon^3 \boldsymbol{Y}_3(T_0, T_2) \tag{13}$$

where the time scales are given by $T_m = \varepsilon^m t$. As shown below, the secular terms appear at the third order and therefore, there is no dependence of the solution on the time scale T_1. Moreover, we set $U = U_f + \varepsilon^2 \sigma_U U_f$, $k_{\alpha 0} = \overline{k_{\alpha 0}} + \varepsilon^2 \sigma_\alpha \overline{k_{\alpha 0}}$, $k_{h0} = \overline{k_{h0}} + \varepsilon^2 \sigma_h \overline{k_{h0}}$, and $k_{ab} = \overline{k_{ab}} + \varepsilon^2 \sigma_\alpha \overline{k_{ab}}$. The aeroelastic response is inspected in the vicinity of the flutter onset. The time derivative is expressed in terms of these scales as [41]

$$\frac{d}{dt} = D_0 + \varepsilon^2 D_2 + \ldots \tag{14}$$

where $D_m = \partial/\partial T_m$. Substituting Eqs. (13) and (14) into Eq. (9) and equating coefficients of like powers of ε, we obtain.

Order (ε):

$$D_0 \boldsymbol{Y}_1 - A(U_f)\boldsymbol{Y}_1 = 0 \tag{15}$$

Order (ε^2):

$$D_0 \boldsymbol{Y}_2 - A(U_f)\boldsymbol{Y}_2 = Q(\boldsymbol{Y}_1, \boldsymbol{Y}_1) \tag{16}$$

Order (ε^3):

$$\begin{aligned} D_0 \boldsymbol{Y}_3 - A(U_f)\boldsymbol{Y}_3 = & -D_2 \boldsymbol{Y}_1 + \sigma_U B_1 \boldsymbol{Y}_1 + \sigma_h B_2 \boldsymbol{Y}_1 \\ & + \sigma_\alpha B_3 \boldsymbol{Y}_1 + \sigma_{ab} B_4 \boldsymbol{Y}_1 \\ & + 2Q(\boldsymbol{Y}_1, \boldsymbol{Y}_2) + C(\boldsymbol{Y}_1, \boldsymbol{Y}_1, \boldsymbol{Y}_1) \end{aligned} \tag{17}$$

where the matrices $B_1 - B_4$ are given in the appendix.

The general solution is the superposition of six linearly independent solutions that correspond to six eigenvalues: two of which are purely imaginary. We keep only the nondecaying solutions and express the general solution of the first-order problem as

$$\boldsymbol{Y}_1 = z(T_2)\boldsymbol{p}e^{i\omega T_0} + \overline{z}(T_2)\overline{\boldsymbol{p}}e^{-i\omega T_0} \tag{18}$$

where the function $z(T_2)$ is determined by imposing the solvability condition [59, 60] at the third order and $\boldsymbol{p}$ is the eigenvector of $A(U_f)$ corresponding to the eigenvalue $i\omega$, that is,

$$A(U_f)\boldsymbol{p} = i\omega\boldsymbol{p} \tag{19}$$

Substituting the $\boldsymbol{Y}_1$ into the second-order expansion yields

$$D_0\boldsymbol{Y}_2 - A(U_f)\boldsymbol{Y}_2 = Q(\boldsymbol{p},\boldsymbol{p})z^2e^{2i\omega T_0} + 2Q(p,\overline{p})z\overline{z} + Q(\overline{\boldsymbol{p}},\overline{\boldsymbol{p}})\overline{z^2}e^{-2i\omega T_0} \tag{20}$$

The solution of the preceding equation can be written according to Nayfeh [43] as

$$\boldsymbol{Y}_2 = \boldsymbol{\zeta}_2 z^2 e^{2i\omega T_0} + 2\boldsymbol{\zeta}_0 z\overline{z} + \overline{\boldsymbol{\zeta}_2 z^2}e^{-2i\omega T_0} \tag{21}$$

where

$$\left[2i\omega I - A(U_f)\right]\zeta_2 = Q(\boldsymbol{p},\boldsymbol{p}) \quad \text{and} \quad A(U_f)\zeta_0 = -Q(\boldsymbol{p},\overline{\boldsymbol{p}}) \tag{22}$$

Substituting the preceding solutions into the third-order expansion, we obtain

$$\begin{aligned} &D_0\boldsymbol{Y}_3 - A(U_f)\boldsymbol{Y}_3 \\ &= -[D_2\boldsymbol{Y}_1 - \sigma_U B_1\boldsymbol{z}\boldsymbol{p} + \sigma_h B_2\boldsymbol{z}\boldsymbol{p} + \sigma_\alpha B_3\boldsymbol{z}\boldsymbol{p} \\ &\quad + \sigma_{ab}B_4\boldsymbol{z}\boldsymbol{p} - (4Q(\boldsymbol{p},\zeta_0) + 2Q(\overline{\boldsymbol{p}},\zeta_2) \\ &\quad + C(\boldsymbol{p},\boldsymbol{p},\overline{\boldsymbol{p}}))z^2\overline{z}]e^{i\omega T_0} + cc + NST \end{aligned} \tag{23}$$

where cc stands for the complex conjugate of the preceding terms and *NST* stands for terms that do not produce secular terms. To determine the solvability condition, we define q as the left eigenvector of $A(U_f)$ corresponding to the eigenvalue $i\omega$, that is,

$$A(U_f)^T\boldsymbol{q} = i\omega\boldsymbol{q} \tag{24}$$

and normalize it so that $\boldsymbol{q}^T\boldsymbol{p} = 1$. Then, the solvability condition requires that terms proportional to $e^{i\omega T_0}$ be orthogonal to $\boldsymbol{q}$. Imposing this condition on the case of a system of equations for a single absorber (without loss of generality), we obtain from *Mathematica* based on the present aeroelastic system specifications the following complex-valued normal form of the Hopf bifurcation:

$$\begin{aligned} D_2z = &[(0.330292 + 0.339775i)\sigma_U U_f \\ &- (0.00117818 - 0.000390227i)\sigma_h k_{h0} \\ &+ (0.273915 + 0.586557i)\sigma_\alpha k_{\alpha 0} \\ &+ (1.99391 + 3.22409i)x10^{-6}\sigma_{ab}k_{ab0}]z \\ &+ [(0.00412655 + 0.00883654i)k_{\alpha_2} \\ &- (0.000504111 + 0.00105577i)k_{\alpha_1}^2 \\ &- (0.000576729 + 0.00123473i)k_{h1}k_{\alpha_1} \\ &+ (0.0000216166 + 0.0000355953i)k_{ab1}k_{\alpha_1} \\ &- (2.76733 - 0.916571i)x10^{-7}k_{h2} \\ &- (9.47654 - 3.13823i)x10^{-8}k_{h1}^2 \\ &+ (0.0000132461 + 0.0000146894i)k_{ab1}k_{h1} \\ &+ (0.0000398153 + 0.0000460757i)k_{ab2} \\ &- (2.22761 + 2.51984i)x10^{-7}k_{ab1} \\ &- (0.0203722 + 0.0224978i)c_s]z^2\overline{z} \end{aligned} \tag{25}$$

For convenience, we write the preceding equation as

$$D_2z = \beta z + \Lambda z^2\overline{z} \tag{26}$$

where

$$\begin{aligned} \mathrm{Re}(\beta) = &\beta_r = [(0.330292)\sigma_U U_f - (0.00117818)\sigma_h k_{h0} \\ &+(0.273915)\sigma_\alpha k_{\alpha 0} + (1.99391)\times 10^{-6}\sigma_{ab}k_{ab0}] \end{aligned} \tag{27a}$$

$$\begin{aligned} \mathrm{Im}(\beta) = &\beta_i = [(0.339775)\sigma_U U_f - (-0.000390227)\sigma_h k_{h0} \\ &+(0.586557)\sigma_\alpha k_{\alpha 0} + (3.22409)\times 10^{-6}\sigma_{ab}k_{ab0}] \end{aligned} \tag{27b}$$

$$\begin{aligned} Re(\Lambda) = &\Lambda_r = \big[(41265.5)k_{\alpha_2} - (5041.11)k_{\alpha_1}^2 \\ &-(5767.29)k_{h1}k_{\alpha_1} + (216.166)k_{ab1}k_{\alpha_1} \\ &-(2.76733)k_{h2} - (0.947654)k_{h1}^2 \\ &+(132.461)k_{ab1}k_{h1} + (398.153)k_{ab2} \\ &-(2.22761)k_{ab1} - (203722)c_s]\times 10^{-7} \end{aligned} \tag{27c}$$

$$\begin{aligned} Im(\Lambda) = &\Lambda_i = \big[(88365.4)k_{\alpha_2} - (10557.7)k_{\alpha_1}^2 \\ &-(12347.3)k_{h1}k_{\alpha_1} + (355.953)k_{ab1}k_{\alpha_1} \\ &-(-0.916571)\times 10^{-7}k_{h2} \\ &-(-.313823)k_{h1}^2 + (146.894)k_{ab1}k_{h1} \\ &+(460.757)k_{ab2} - (2.51984)k_{ab1} - (224978)c_s]\times 10^{-7} \end{aligned} \tag{27d}$$

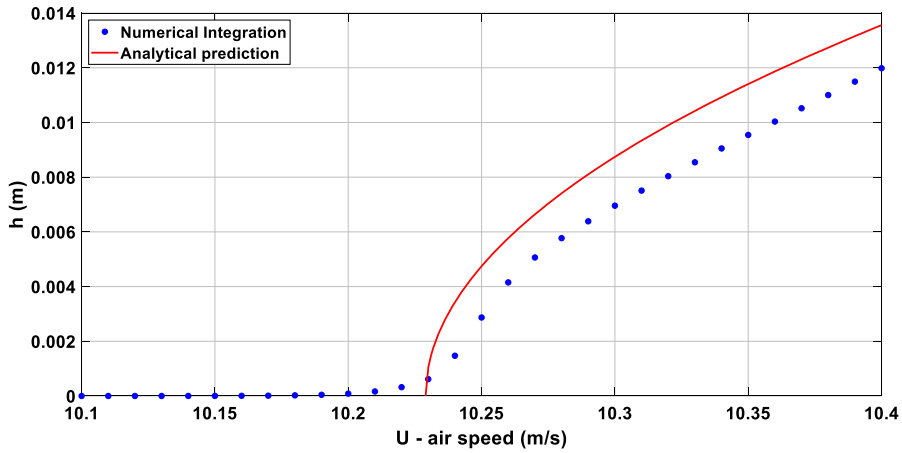

(a) Plunging motion

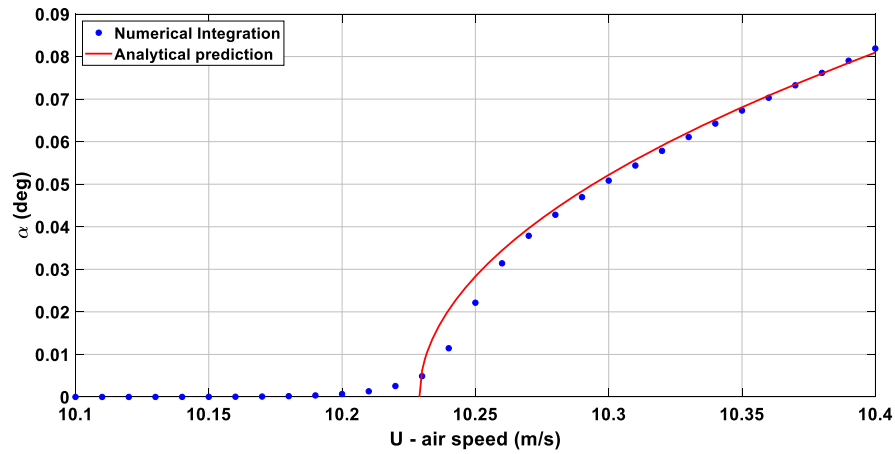

(b) Pitching motion

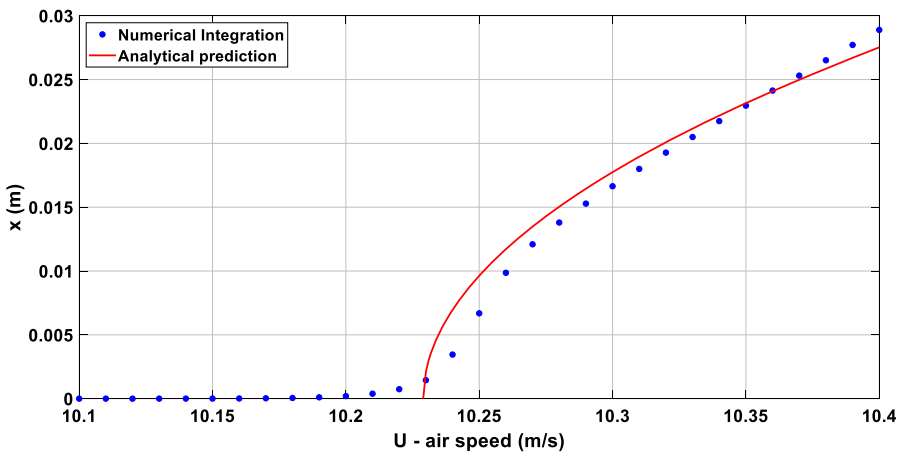

(c) Vibration absorber motion

Fig. 11 Amplitude of the limit cycle oscillations: analytical vs. numerical solutions

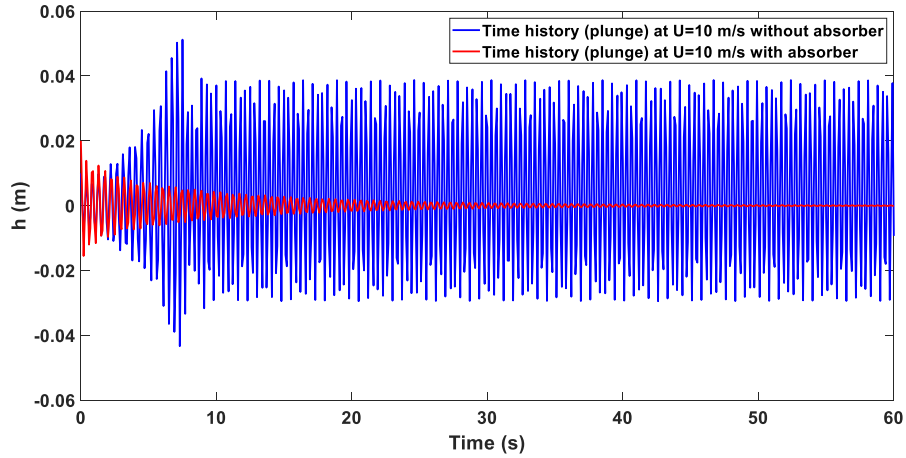

(a) Plunging motion

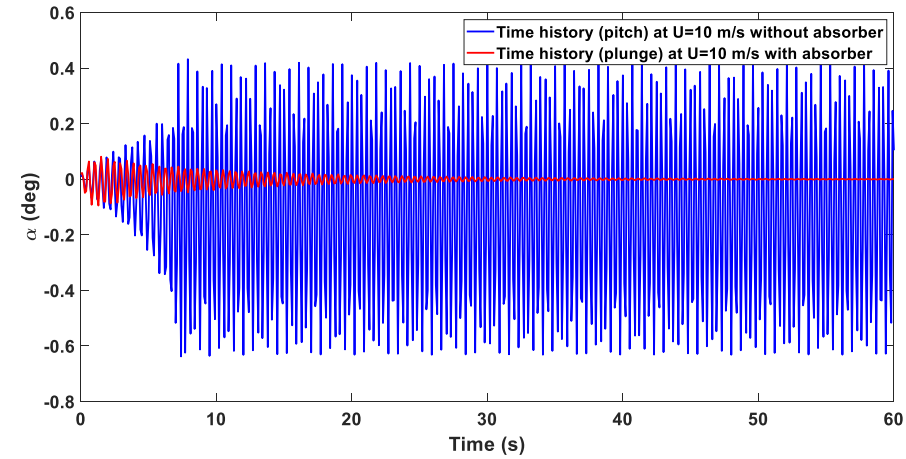

(b) Pitching motion

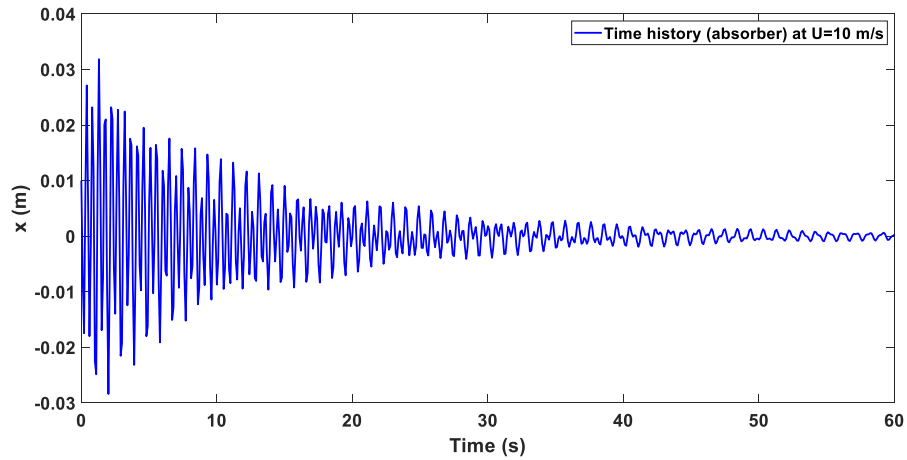

(c) Vibration absorber motion

Fig. 12 Dynamic response of the aeroelastic system at U = 10 m/s (with and without absorber)

and *Re* and *Im* stand for the real and imaginary parts, respectively.

Next, we consider the polar form by letting $z = \frac{1}{2} r e^{i\theta}$ and separate the real and imaginary parts. We obtain three equilibrium solutions for the r component, namely

$$r = 0, r = \pm\sqrt{\frac{-4\beta_r}{\Lambda_r}} \tag{28}$$

3.4 Parametric study

In order to check the accuracy of the analytical formulation given by the normal form in predicting the amplitude of the LCOs, we consider the case in which structural nonlinearity is applied only in the pitch degree of freedom, that is $k_{h0} = 2844.4$, $k_{\alpha 0} = 6.833$, $k_{\alpha_1} = 29.996$, $k_{\alpha_2} = 67.685$, $k_{h1} = k_{h2} = k_{ab1} = k_{ab2} = c_s = 0$ [3]. The absorber specifications are given in Table 2. The amplitude of the LCO of each degree of freedom is given by

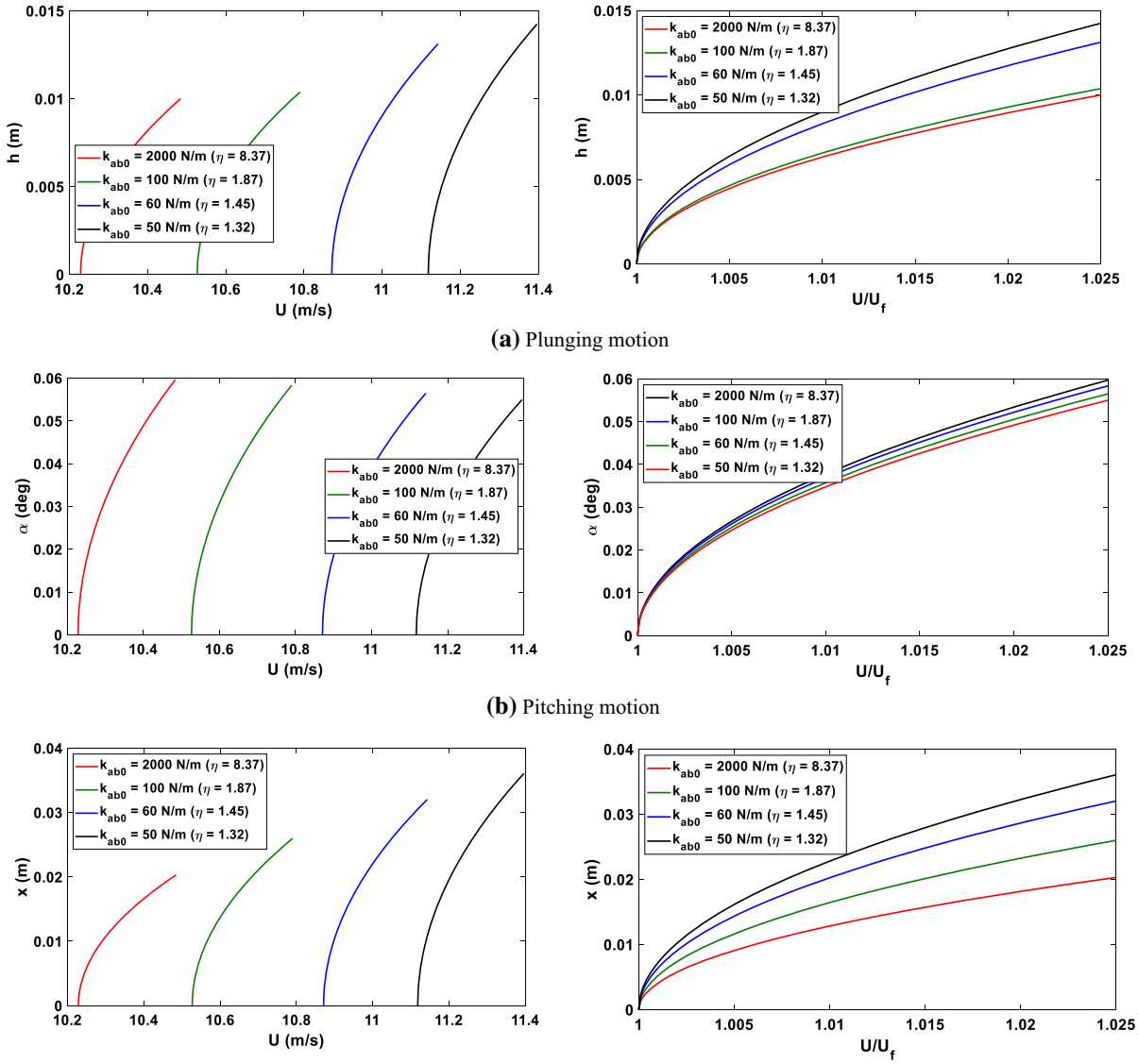

(a) Plunging motion

(b) Pitching motion

(c) Vibration absorber motion

Fig. 13 Bifurcation diagrams obtained for different linear stiffness coefficients of the absorber

$$A_h = r\sqrt{\boldsymbol{p}1_r^2 + \boldsymbol{p}1_i^2}$$
$$A_\alpha = r\sqrt{\boldsymbol{p}2_r^2 + \boldsymbol{p}2_i^2} \quad (29)$$
$$A_x = r\sqrt{\boldsymbol{p}3_r^2 + \boldsymbol{p}3_i^2}$$

where $\boldsymbol{p}j_r$ and $\boldsymbol{p}j_i$ denote the real and imaginary parts of the j-*th* component of the vector $\boldsymbol{p}$, respectively. In Fig. 11a–c, we plot the LCO amplitudes for the pitch, plunge and vibration absorber motions obtained from the numerical integration of the original governing equations and the normal form. The numerical and analytical results in Fig. 11a–c show that the system with the given parameters experiences a delay in the flutter onset, in comparison with the case without absorber, and operates in the supercritical regime, as manifested by the smooth occurrence of limit cycle oscillations at the flutter speed predicted from the linear analysis. The incorporation of a passive absorber to the present aeroelastic system enabled an increase in the flutter speed while maintaining the supercritical post-flutter behavior. This indicates a safe operation of the aeroelastic system when equipped with a vibration absorber. On the other hand, Malher et al. [42] observed a shift from supercritical to subcritical behavior when adding a vibration absorber. Furthermore, they obtained large LCO amplitudes in the plunge mode, which constitute a weakness in the design. The analytical results show a good agreement with their numerical counterparts near the Hopf bifurcation. The verification of the analytical results enables to conduct a parametric study to investigate the impact of the vibration absorber on the nonlinear response beyond the flutter.

To illustrate the effect of the absorber parameters on the dynamic behavior of the aeroelastic system, we generate the time histories of its motions along all degrees of freedom at a fixed air speed with and without vibration absorber. The results obtained from the numerical integration are displayed in Fig. 12. Figure 12a, b shows the time histories of the plunge and pitch motions with and without vibration absorber at a relative high speed which is 10 m/s. These figures show the effect of the absorber in suppressing the oscillations at high speed. We note that this speed ($U = 10\,\mathrm{m/s}$) is lower than the flutter speed of the system embedded with an absorber, as per the previous linear analysis. Therefore, the plunge and pitch motion in the second case (with the absorber) show no oscillation after some time. This decay in amplitude of plunge and pitch is compensated by the oscillation of the absorber shown in Fig. 12c. Here after some time, the absorber still experiences some oscillations which explains how the energy of the system is transferred to the absorber. Given the computational time associated with the numerical integration and the verification of the normal form as shown above, we proceed with the parametric study using the analytical formulation.

Table 4 Vibration absorber specifications for the three cases under investigation

	Case I	Case II	Case III
k_{ab0}(N/m)	50	0.5	50
l	1.25	0.5	1.25
c_{ab}(Kg/s)	0.01	0.01	0.001

The analytical form of solution enables to examine several case studies with targeted values according to the nonlinear coefficients obtained in the normal form. Firstly, the parametric study of the linear stiffness coefficient of the vibration absorber is investigated and the analysis is expanded to include the nonlinear coefficients. We show in Fig. 13 the effect of varying the linear coefficient of stiffness of the absorber on the amplitude of LCOs. As shown in the linear analysis, decreasing the stiffness shifts the flutter speed to higher values. However, this improvement is observed to come at the expense of an increase in the amplitude of the LCO as can be shown in the figures presented in the left frame in which the results are given in terms of the normalized speed $\frac{U}{U_f}$. The results show that the linear stiffness coefficient that results in the highest flutter speed ($k_{ab0} = 50\mathrm{N/mor}\eta = 1.32$) also leads to the highest LCO amplitude beyond flutter when compared to the other stiffness coefficient values. This indicates that despite the improvement in terms of flutter delay, a bifurcation diagram with a higher slope is obtained when adding the vibration absorber, which in turn gives a higher amplitude of limit cycle oscillations.

Next, we investigate the effect of the nonlinear stiffness coefficients of the vibration absorber. Three different case studies are considered. In each case, damping coefficient or the position of the absorber or both are changed and the linear coefficient of the

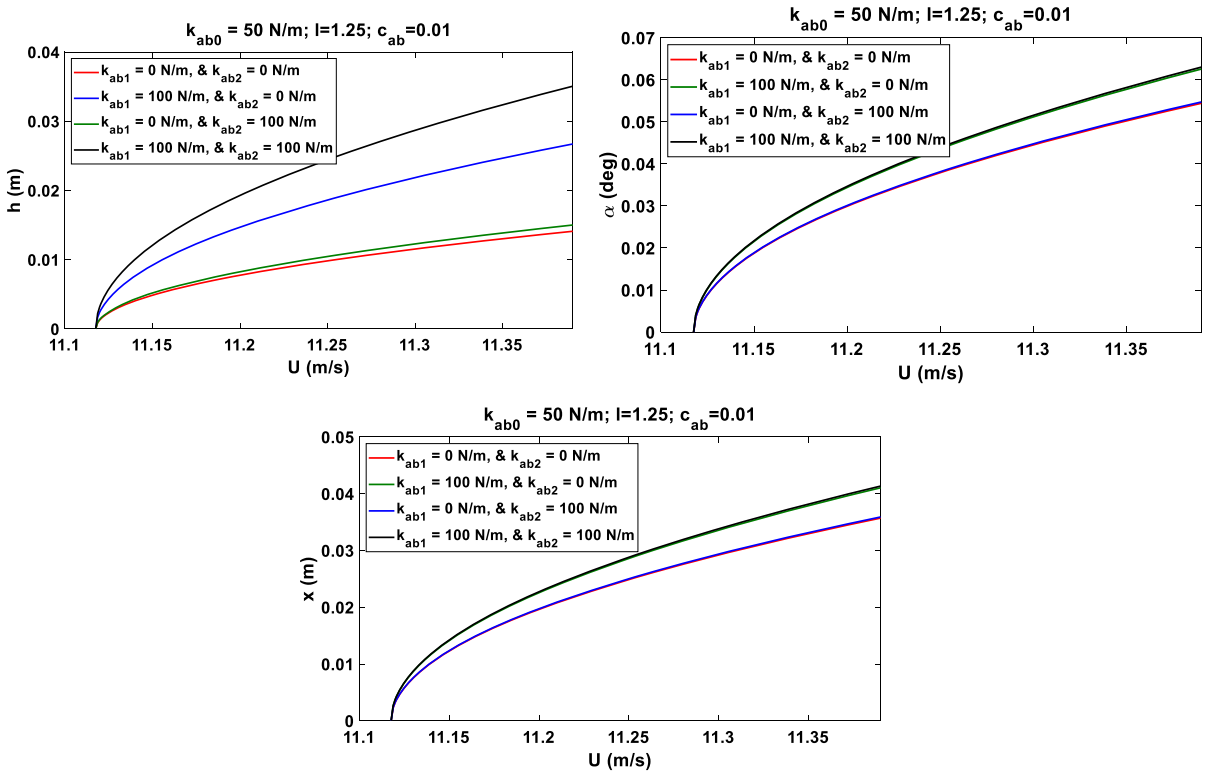

Fig. 14 Bifurcation diagrams of the plunging, pitching, and vibration absorber motions (Case I)

stiffness is kept constant. For all three cases, the quadratic and cubic nonlinearities of the absorber were changed separately and/or together to observe their effect. These cases are summarized in Table 4.

Inspecting cases I, II and III, it is noticed that the flutter speed at which the Hopf bifurcation occurs is different given the selected parameters of the vibration absorber: k_{ab0}, c_{ab} and l. As expected, the variations in the nonlinear coefficients do not affect the onset of flutter, unless the aeroelastic system shifts from supercritical to subcritical behavior. We show in Figs. 14, 15 and 16 the bifurcation diagrams obtained for different values of the nonlinear stiffness coefficients. Of interest for all cases, we observe that the lowest amplitudes of the LCOs are achieved when setting the quadratic and cubic nonlinearities of the vibration absorber stiffness equal to zero (as shown by the red curves). Incorporating nonlinear stiffness coefficients is always observed to degrade the aeroelastic system by amplifying the amplitude of the LCOs beyond flutter. Inspecting the dynamic response of the system (plunge, pitch and vibration absorber motions), as shown in Figs. 14, 15 and 16, no improvement is observed by adding cubic or quadratic nonlinearities to the vibration absorber's stiffness. The degrading impact of the nonlinear terms of the absorber can be also predicted from the nonlinear coefficient of the normal form. Based on the configuration of the present aeroelastic system [3], the incorporation of k_{ab1} and k_{ab2} leads to a decrease in the nonlinear coefficient Λ_r, which results in an increase in the amplitude of LCO.

Another point which is worth to note is that the absorber tends to have a larger motion when compared to the plunge motion of the aeroelastic system, as shown in Figs. 10, 11, and 12. This is expected since the vibration absorption mechanism is based on the transfer of energy from the main structure to the absorber.

To gain more insight into the combined effect of the quadratic and cubic stiffness coefficients of the vibration absorber on the type of instability, we generate a contour plot showing variations of Λ_r with k_{ab1} and k_{ab2}. The sign of this coefficient is indicative of the response regime: supercritical (safe behavior) or subcritical (catastrophic behavior). The contour plot in Fig. 17 reveals the range of values for k_{ab1} and k_{ab2} and

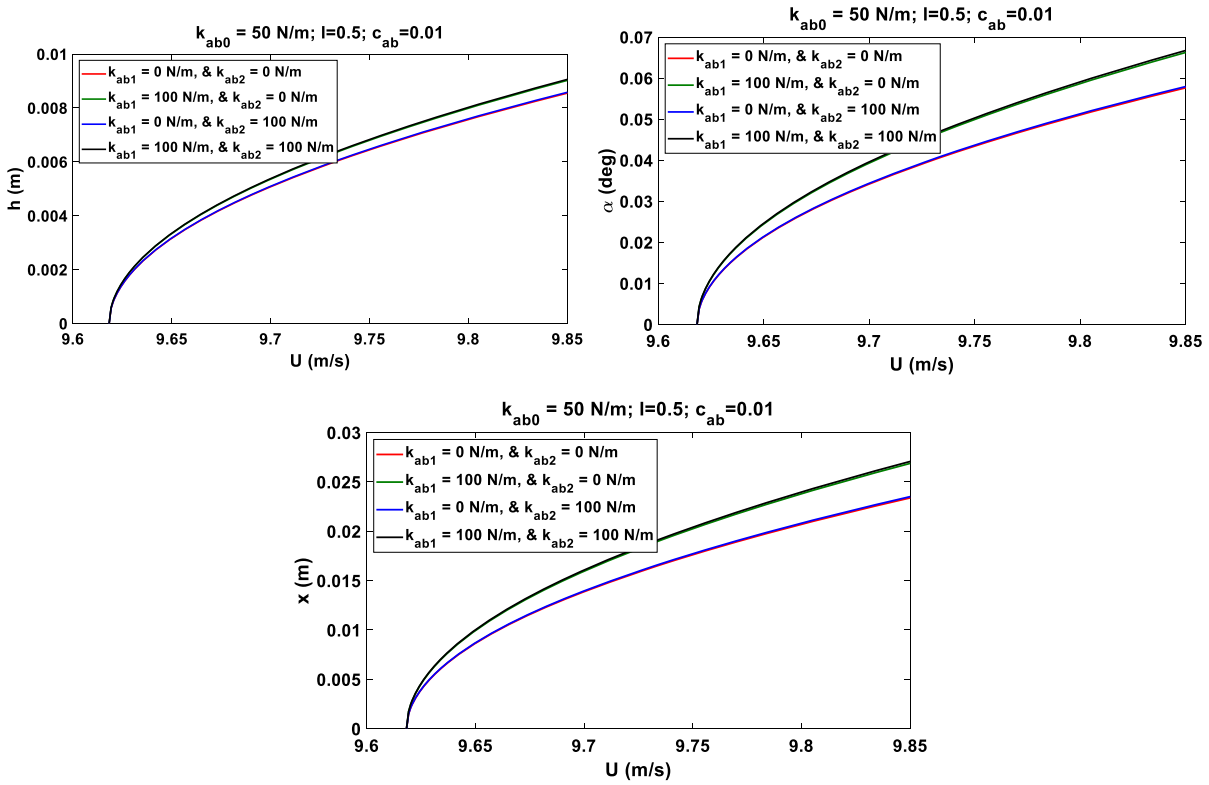

Fig. 15 Bifurcation diagrams of the plunging, pitching, and vibration absorber motions (Case II)

that lead to supercritical response regime, which enables smooth transition to decaying dynamic solution to limit cycle oscillations, unlike the subcritical behavior characterized by abrupt jump to large-amplitude dynamic response.

3.5 Soft pitch springs

In this section, the influence of the absorber on the airfoil with a soft pitch spring is investigated. According to Petit and Beran [61], cubic and quintic terms in the restoring moment associated with the pitching motion are representative of soft springs. As such, the restoring moment is expressed in the form of

$$k_\alpha(\alpha) = k_{\alpha 0} + k_{\alpha 1}\alpha + k_{\alpha 2}\alpha^2 + k_{\alpha 4}\alpha^4 \tag{30}$$

Subsequently, the state space form of the equations of motion is updated, and the nonlinear part of the compact form is adjusted to include the new quintic term. The new nonlinear terms in Eq. (11) are adjusted as follows:

$$NL'^{(Y^2,Y^3,Y^5)} = NL(\boldsymbol{Y}^2, \boldsymbol{Y}^3) + NL(\boldsymbol{Y}^5) \tag{31}$$

where $NL(\boldsymbol{Y}^5)$ is

$$\begin{pmatrix} 0 \\ 0 \\ 0 \\ \dfrac{(bm_w x_\alpha k_{\alpha 4})}{d} * Y_2^5 \\ -\dfrac{(m_T k_{\alpha 4})}{d} * Y_2^5 \\ 0 \end{pmatrix}$$

For the sake of comparison with its linear and hard springs counterparts, the optimal case of a single absorber is solved numerically for all three cases and their bifurcation diagrams are shown in Fig. 18. This figure shows a noticeable effect of the spring characteristics on the post-flutter behavior. The linear pitch spring shows a divergent oscillatory behavior. This is expected as the aeroelastic system relies primarily on the structural nonlinearities to trigger the limit cycle oscillations beyond flutter. For the hard spring case, the nonlinear coefficients of the pitch spring are

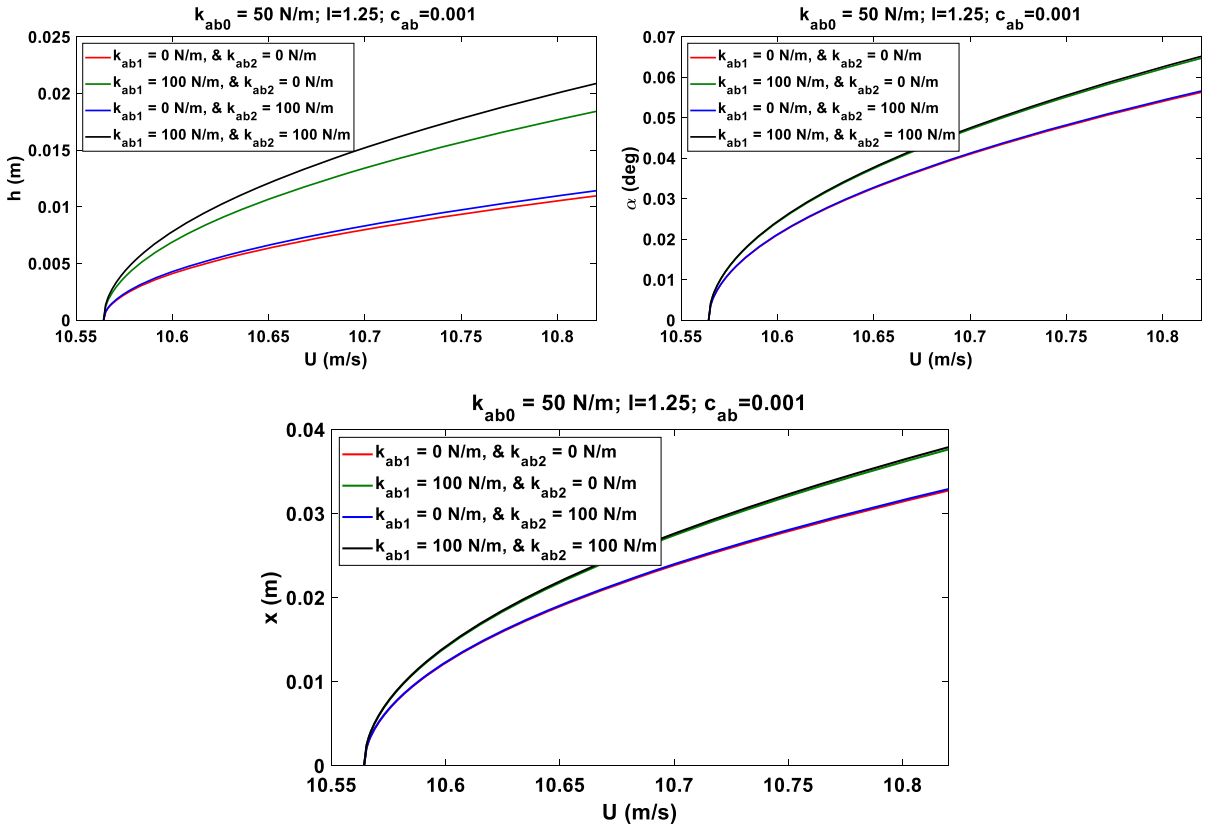

Fig. 16 Bifurcation diagrams of the plunging, pitching, and vibration absorber motions (Case III)

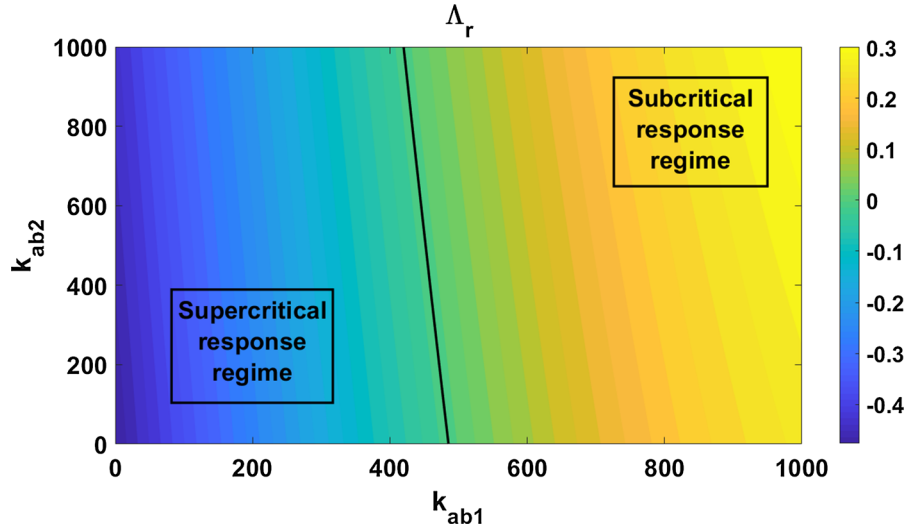

Fig. 17 Contour plot of real part of the nonlinear coefficient of the normal form Λ vs. the quadratic and cubic coefficients of the vibration absorber's stiffness

chosen to be $k_{\alpha 1} = 29.996$ N/m and $k_{\alpha 2} = 65.4$ N/m in compliance to the parametric study shown earlier and according the previously published studies [3, 44]. On the other hand, for the soft springs, the quintic coefficient $k_{\alpha 4}$ is set equal to 7 N/m and the cubic coefficient $k_{\alpha 2}$ is equal to –65.4 N/m. As shown in Fig. 18, the limit cycle oscillations of the plunge, pitch and absorber motions are significantly mitigated in

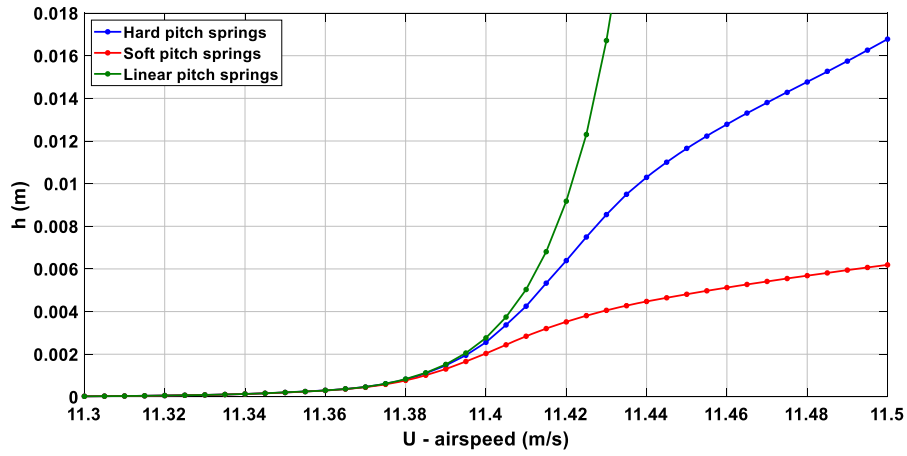

(a) Plunging motion

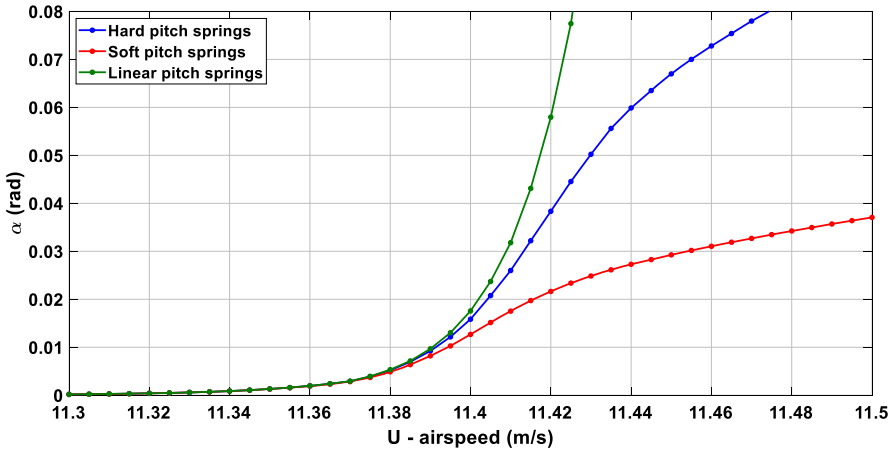

(b) Pitching motion

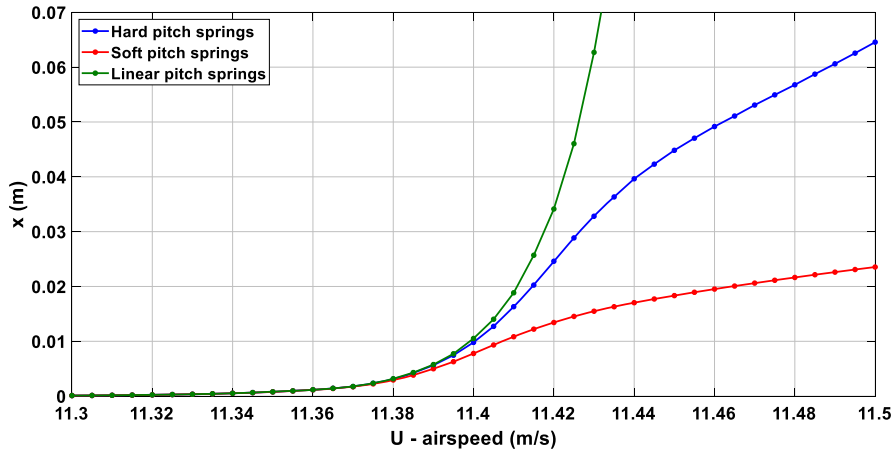

(c) Vibration absorber motion

Fig. 18 Bifurcation diagrams obtained for soft, hard and linear pitch springs

comparison with the nonlinear behavior obtained for hard springs. Moreover, the supercritical behavior is maintained in the post-critical regime. Malher et al. [42] reported also attractive cases with soft pitch

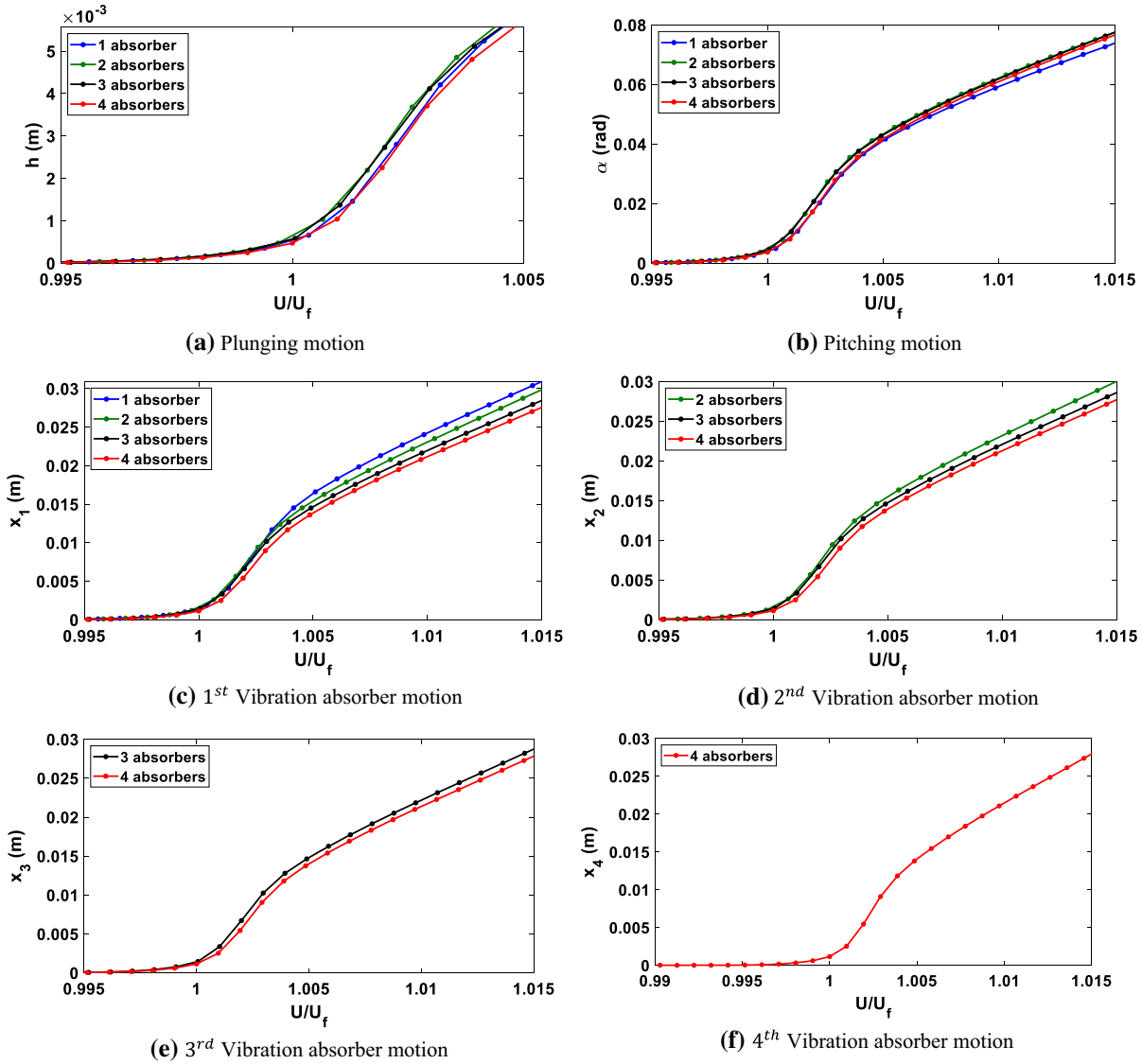

(a) Plunging motion

(b) Pitching motion

(c) 1^{st} Vibration absorber motion

(d) 2^{nd} Vibration absorber motion

(e) 3^{rd} Vibration absorber motion

(f) 4^{th} Vibration absorber motion

Fig. 19 Nondimensionalized bifurcation diagrams obtained for different number of absorbers with a constant stiffness (100 N/m)

springs for the control of the flutter onset and post-flutter behavior. However, soft springs remain more difficult to implement and handle in comparison with their hard counterparts [42].

3.6 Post-flutter response of metastructure aeroelastic system

Similar to the linear analysis, we investigate the effect of deploying an array of distributed vibration absorbers on the post-flutter regime. The linear analysis of the metastructure revealed that increasing the number of vibration absorbers while properly selecting their stiffness is beneficial in terms of delaying the occurrence of flutter. Apart from this advantage, the metastructure shows another benefit in the post-flutter regime. A single absorber normally oscillates at a higher amplitude than its counterpart multiple absorbers. This is because the entire mechanical energy is dissipated through only one absorber rather than being split among multiple absorbers. To gain an insight of this advantage, the flutter speed is nondimensionalized by its respective flutter speed and the bifurcation diagrams obtained for different number of vibration

absorbers are presented in Fig. 19. We note that the stiffness of all absorbers is kept constant and equal to $k_{ab} = 100$ N/m for all simulation cases shown in Fig. 19. We observe that the use of more absorbers leads to lower LCO amplitude beyond the flutter. The speed is nondimensionalized since the flutter speed varies when altering the number of vibration absorbers. Figure 19 depicts an improvement in the system's performance when deploying multiple absorber, especially for the plunge mode. For instance, at a speed ratio $\frac{U}{U_f}$ of 1.01, equipping the aeroelastic system with four absorbers results in an amplitude of LCO of the plunge motion of 2 cm. On the other hand, the use of a single absorber leads to an amplitude of 3 cm. Furthermore, the use of multiple resonators enables a better distribution of the mechanical energy being absorbed and thus, the amplitude of oscillations of each absorber is decreased as demonstrated in Fig. 19c–f.

4 Conclusions

This work examined the control of the flutter onset in aircraft wings and the suppression of their induced vibrations using a conserved-mass metastructure. The mitigation mechanism is based on a passive vibration absorption concept. We considered a rigid airfoil supported by nonlinear springs in the pitch and plunge directions, equipped with an array of cantilever beams with a tip mass acting as vibration absorbers, and subjected to nonlinear aerodynamic loads. We first conducted a linear analysis to study the effect of absorbers' parameters on the flutter speed. These include the number of vibration absorbers, their stiffness, damping and position with respect to the elastic axis. We found that a combination of these parameters may lead to a degrading performance when compared to the system without absorber. On the other hand, a proper selection of the aforementioned parameters enabled an increase of 23.4% in the flutter speed when deploying a single vibration absorber. The study showed that a choice of the absorber's stiffness of 46.5N/m, corresponding to a frequency ratio associated with the plunging and absorber motions of 1.3, leads to the highest flutter speed. Moreover, we observed that the closer the absorber is to the leading edge, the better performance it exhibits, and the flutter onset is noticeably delayed for the same stiffness and damping values. Our numerical study revealed that increasing the number of vibration absorbers while properly selecting their stiffness is beneficial in terms of delaying the occurrence of flutter. It was found that a selection of four absorbers with a stiffness of 9.23 N/m resulted in an 84% increase in the flutter speed with respect to the aeroelastic system without absorbers.

The method of multiple scales was used to develop the normal form of the aeroelastic system equipped with the vibration absorbers to analyze its nonlinear dynamic behavior beyond flutter. The analytical reduced-order model was verified against the numerical integration of the governing equations. The normal form enables to investigate the limit cycle oscillation (LCOs) beyond the flutter speed (Hopf bifurcation) with much lower computational requirements compared to the numerical integration. The nonlinear analysis verified that decreasing the linear stiffness of the absorber delays the flutter onset. However, this comes at the expense of a higher LCO amplitude beyond flutter. Moreover, it was found that incorporating quadratic and cubic stiffness coefficients to the absorber degrades the aeroelastic system by amplifying the amplitude of LCOs beyond flutter. The use of soft pitch spring was observed to be better than its hard counterpart in terms of controlling the supercritical post-flutter behavior as it leads to lower LCO amplitudes for both pitch and plunge modes. Equipping the aeroelastic system with multiple absorbers was also beneficial in terms of controlling the post-flutter regime.

The sensitivity analysis presented here is a first step toward the design and development of an optimal control system for vibration mitigation of aircraft wings. Optimization studies of the spatial collocation of vibration absorbers and the effectiveness of distributed hysteretic vibration absorbers for aircraft wings can be considered as future work.

Acknowledgements The author M. Ghommem gratefully acknowledges the financial support via the American University of Sharjah Faculty research grant FRG19-M-E26 (fund number EN6001).

Data Availability The data that support the findings of this study are available from the corresponding author upon reasonable request.

Declarations

Conflict of interest The authors declare that they have no conflict of interest.

Appendix

The notations presented in Eq. (17) are expressed as:

$$B_1 = -2U_f^2(k_1 I_1 + k_2 I_2) \qquad B_2 = \overline{k_{h0}}(c_1 I_3 + c_2 I_4)$$

$$B_3 = \overline{k_{\alpha 0}}(c_5 I_5 + c_6 I_6) \qquad B_4 = \overline{k_{ab0}}(c_6 I_7 + c_7 I_8 + c_8 I_9)$$

$$I_1 = \begin{pmatrix} 0&0&0&0&0&0\\ 0&0&0&0&0&0\\ 0&0&0&0&0&0\\ 0&1&0&1&1&0\\ 0&0&0&0&0&0\\ 0&0&0&0&0&0 \end{pmatrix} \quad I_2 = \begin{pmatrix} 0&0&0&0&0&0\\ 0&0&0&0&0&0\\ 0&0&0&0&0&0\\ 0&0&0&0&0&0\\ 0&1&0&1&1&0\\ 0&0&0&0&0&0 \end{pmatrix}$$

$$I_3 = \begin{pmatrix} 0&0&0&0&0&0\\ 0&0&0&0&0&0\\ 0&0&0&0&0&0\\ 1&0&0&0&0&0\\ 0&0&0&0&0&0\\ 0&0&0&0&0&0 \end{pmatrix} \quad I_4 = \begin{pmatrix} 0&0&0&0&0&0\\ 0&0&0&0&0&0\\ 0&0&0&0&0&0\\ 0&0&0&0&0&0\\ 1&0&0&0&0&0\\ 0&0&0&0&0&0 \end{pmatrix}$$

$$I_5 = \begin{pmatrix} 0&0&0&0&0&0\\ 0&0&0&0&0&0\\ 0&0&0&0&0&0\\ 0&1&0&0&0&0\\ 0&0&0&0&0&0\\ 0&0&0&0&0&0 \end{pmatrix} \quad I_6 = \begin{pmatrix} 0&0&0&0&0&0\\ 0&0&0&0&0&0\\ 0&0&0&0&0&0\\ 0&0&0&0&0&0\\ 0&1&0&0&0&0\\ 0&0&0&0&0&0 \end{pmatrix}$$

$$I_7 = \begin{pmatrix} 0&0&0&0&0&0\\ 0&0&0&0&0&0\\ 0&0&0&0&0&0\\ 1&1&1&0&0&0\\ 0&0&0&0&0&0\\ 0&0&0&0&0&0 \end{pmatrix} \quad I_8 = \begin{pmatrix} 0&0&0&0&0&0\\ 0&0&0&0&0&0\\ 0&0&0&0&0&0\\ 0&0&0&0&0&0\\ 1&1&1&0&0&0\\ 0&0&0&0&0&0 \end{pmatrix}$$

$$I_9 = \begin{pmatrix} 0&0&0&0&0&0\\ 0&0&0&0&0&0\\ 0&0&0&0&0&0\\ 0&0&0&0&0&0\\ 0&0&0&0&0&0\\ 1&1&1&0&0&0 \end{pmatrix}$$

References

1. Lee, B., Jiang, L., Wong, Y.: Flutter of an airfoil with a cubic nonlinear restoring force. In 39th AIAA/ASME/ASCE/AHS/ASC Structures, Structural Dynamics, and Materials Conference and Exhibit (1998).
2. Chabalko, C., Hajj, M., Mook, D., Silva, W.: Characterization of the LCO Response behaviors of the NATA model. In 47th AIAA/ASME/ASCE/AHS/ASC Structures, Structural Dynamics, and Materials Conference 14th AIAA/ASME/AHS Adaptive Structures Conference 7th (2006).
3. Ghommem, M., Hajj, M.R., Nayfeh, A.H.: Uncertainty analysis near bifurcation of an aeroelastic system. J. Sound Vib. **329**(16), 3335–3347 (2010)
4. Sanches, L., Guimarães, T.A.M., Marques, F.D.: Aeroelastic tailoring of nonlinear typical section using the method of multiple scales to predict post-flutter stable LCOs. Aerosp. Sci. Technol. **90**, 157–168 (2019)
5. Abdelkefi, A., Ghommem, M., Nuhait, A.O., Hajj, M.R.: Nonlinear analysis and enhancement of wing-based piezoaeroelastic energy harvesters. J. Sound Vib. **333**(1), 166–177 (2014)
6. Hayat, K., Ha, S.K.: Flutter performance of large-scale wind turbine blade with shallow-angled skins. Compos. Struct. **132**, 575–583 (2015)
7. Griffin, D., Zuteck, M.: Scaling of composite wind turbine blades for rotors of 80 to 120 meter diameter. In 20th 2001 ASME Wind Energy Symposium (2001).
8. Basta, E., Ghommem, M., Romdhane, L., Abdelkafi, A.: Modeling and experimental comparative analysis on the performance of small-scale wind turbines. Wind Struct. **30**(3), 261–273 (2020)
9. Robinett, R.D., Wilson, D.G.: Maximizing the performance of wind turbines with nonlinear aeroservoelastic power flow control. In 2010 IEEE International Conference on Control Applications (2010).
10. Berci, M., Mascetti, S., Incognito, A., Gaskell, P.H., Toropov, V.V.: Gust response of a typical section via CFD and analytical solutions. In V European Conference on Computational Fluid Dynamics (2010).
11. Hübner, B., Walhorn, E., Dinkler, D.: A monolithic approach to fluid–structure interaction using space–time finite elements. Comput. Methods Appl. Mech. Eng. **193**(23–26), 2087–2104 (2004)
12. Borri, C., Costa, C., Zahlten, W.: Non-stationary flow forces for the numerical simulation of aeroelastic instability of bridge decks. Comput. Struct. **80**(12), 1071–1079 (2002)
13. Yang, Z.C., Zhao, L.C.: Analysis of limit cycle flutter of an airfoil in incompressible flow. J. Sound Vib. **123**(1), 1–13 (1988)
14. Weisshaar, T.A.: Divergence of forward swept composite wings. J. Aircr. **17**(6), 442–448 (1980)
15. Farmer, M.: A two-degree-of-freedom flutter mount system with low damping for testing rigid wings at different angles of attack. In NASA Technical Memorandum, vol. NASA-TM-83302, p. 24 (1982).
16. Hansen, M.H.: Aeroelastic instability problems for wind turbines. Wind Energy **10**(6), 551–577 (2007)
17. De Marqui Junior, C., Rebolho, D.C., Belo, E.M., Marques, F.D.: Identification of flutter parameters for a wing model. J. Braz. Soc. Mech. Sci. Eng. **28**(3), 2006.
18. Asjes, D., Diwadkar, A., Vaidya, U., Kelkar, A., Vogel, J.M., Chaussee, D.: Modeling and analysis of rotational freeplay nonlinearity of a 2D airfoil. In 2014 American control conference (2014).

19. Liu, J.-K., Zhao, L.-C.: Bifurcation analysis of airfoils in incompressible flow. J. Sound Vib. **154**(1), 117–124 (1992)
20. Dowell, E., Edwards, J., Strganac, T.: Nonlinear Aeroelasticity. J. Aircr. **40**(5), 857–874 (2003)
21. Woolston, D.S., Runyan, H.L., Andrews, R.E.: An investigation of effects of certain types of structural nonlinearities on wing and control surface flutter. J. Aeronaut. Sci. **24**(1), 57–63 (1957)
22. Shen, S.F.: An approximate analysis of nonlinear flutter problems. J. Aerospace Sci. **26**(1), 25–32 (1959)
23. Balakrishnan, A.V.: Aeroelasticity: the continuum theory. Springer, New York (2012)
24. Hodges, D.H., and Pierce, G.A.: Introduction to Structural Dynamics and Aeroelasticity, vol. 15 (2011).
25. Lee, B.H.K., Price, S.J., Wong, Y.S.: Nonlinear aeroelastic analysis of airfoils: bifurcation and chaos. Prog. Aerosp. Sci. **35**(3), 205–334 (1999)
26. O'Neil, T., Strganac, T.W.: Aeroelastic response of a rigid wing supported by nonlinear springs. J. Aircr. **35**(4), 616–622 (1998)
27. Price, S., Alighanbari, H., Lee, B.: The aeroelastic response of a two-dimensional airfoil with bilinear and cubic structural nonlinearities. In 35th Structures, Structural Dynamics, and Materials Conference (1994).
28. Strganac, T., Ko, J., Thompson, D., Kurdila, A.: Identification and control of limit cycle oscillations in aeroelastic systems. In 40th Structures, Structural Dynamics, and Materials Conference and Exhibit (1999).
29. Shahrzad, P., Mahzoon, M.: Limit cycle flutter of airfoils in steady and unsteady flows. J. Sound Vib. **256**(2), 213–225 (2002)
30. Dimitriadis, G., Vio, G., Cooper, J.: Application of higher-order harmonic balance to non-linear aeroelastic systems. In: 47th AIAA/ASME/ASCE/AHS/ASC Structures, Structural Dynamics, and Materials Conference 14th AIAA/ASME/AHS Adaptive Structures Conference 7th, (2006)
31. Liu, G., Lv, Z.R., Liu, J.K., Chen, Y.M.: Quasi-periodic aeroelastic response analysis of an airfoil with external store by incremental harmonic balance method. Int. J. Non-Linear Mech. **100**, 10–19 (2018)
32. Peretz, O., Gat, A.D.: Forced vibrations as a mechanism to suppress flutter—An aeroelastic Kapitza's pendulum. J. Fluids Struct. **85**, 138–148 (2019)
33. Gilliatt, H.C., Strganac, T.W., Kurdila, A.J.: An Investigation of Internal Resonance in Aeroelastic Systems. Nonlinear Dyn. **31**(1), 1–22 (2003)
34. Wang, D., Chen, Y., Wiercigroch, M., Cao, Q.: Bifurcation and dynamic response analysis of rotating blade excited by upstream vortices. Appl. Math. Mech. **37**(9), 1251–1274 (2016)
35. Gao, G., Zhu, L.: Nonlinearity of mechanical damping and stiffness of a spring-suspended sectional model system for wind tunnel tests. J. Sound Vib. **355**, 369–391 (2015)
36. Nayfeh, A.H., Ghommem, M., Hajj, M.R.: Normal form representation of the aeroelastic response of the Goland wing. Nonlinear Dyn. **67**(3), 1847–1861 (2011)
37. Beran, P.S., Strganac, T.W., Kim, K., Nichkawde, C.: Studies of store-induced limit-cycle oscillations using a model with full system nonlinearities. Nonlinear Dyn. **37**(4), 323–339 (2004)
38. Theodorsen, T., Mutchler, W.: General Theory of Aerodynamic Instability and the Mechanism of Flutter; NACA: Langley Field, VA, USA (1935)
39. Muturi, N., Spies, A.C., Bender, K. Lee, C.L.: Stall flutter oscillation measurements from a two degree-of-freedom airfoil with nonlinear stiffness. In: 54th AIAA/ASME/ASCE/AHS/ASC Structures, Structural Dynamics, and Materials Conference (2013).
40. Tsushima, N., Su, W.: Flutter suppression for highly flexible wings using passive and active piezoelectric effects. Aerosp. Sci. Technol. **65**, 78–89 (2017)
41. Kassem, M., Yang, Z., Gu, Y., Wang, W., Safwat, E.: Active dynamic vibration absorber for flutter suppression. J. Sound Vib. **469**, 115110 (2020)
42. Verstraelen, E., Habib, G., Kerschen, G., Dimitriadis, G.: Experimental passive flutter suppression using a linear tuned vibration absorber. AIAA J. **55**(5), 1707–1722 (2017)
43. Yang, F., Sedaghati, R., Esmailzadeh, E.: Vibration suppression of structures using tuned mass damper technology: A state-of-the-art review. J. Vib. Control, p. 1077546320984305 (2021)
44. Casalotti, A., Arena, A., Lacarbonara, W.: Mitigation of post-flutter oscillations in suspension bridges by hysteretic tuned mass dampers. Eng. Struct. **69**, 62–71 (2014)
45. Bakis, K.N., Massaro, M., Williams, M.S., Graham, J.M.R.: Passive control of bridge wind-induced instabilities by tuned mass dampers and movable flaps. J. Eng. Mech. **143**(9), 04017078 (2017)
46. Kwon, S.D., Park, K.S.: Suppression of bridge flutter using tuned mass dampers based on robust performance design. J. Wind Eng. Ind. Aerodyn. **92**(11), 919–934 (2004)
47. Fitzgerald, B., Sarkar, S., Staino, A.: Improved reliability of wind turbine towers with active tuned mass dampers (ATMDs). J. Sound Vib. **419**, 103–122 (2018)
48. Stewart, G.M., Lackner, M.A.: The impact of passive tuned mass dampers and wind–wave misalignment on offshore wind turbine loads. Eng. Struct. **73**, 54–61 (2014)
49. Fitzgerald, B., Basu, B., Nielsen, S.R.: Active tuned mass dampers for control of in-plane vibrations of wind turbine blades. Struct. Control. Health Monit. **20**(12), 1377–1396 (2013)
50. Lu, Z., Wang, D., Masri, S.F., Lu, X.L.: An experimental study of vibration control of wind-excited high-rise buildings using particle tuned mass dampers. Smart Struct. Syst **18**(1), 93–115 (2016)
51. Basta, E., Ghommem, M., Emam, S.: Vibration suppression of nonlinear rotating metamaterial beams. Nonlinear Dyn. **101**(1), 311–332 (2020)
52. Carboni, B., Lacarbonara, W.: Nonlinear vibration absorber with pinched hysteresis: theory and experiments. J. Eng. Mech. **142**(5), 04016023 (2016)
53. Habib, G., Kádár, F., Papp, B.: Impulsive vibration mitigation through a nonlinear tuned vibration absorber. Nonlinear Dyn. **98**(3), 2115–2130 (2019)
54. Basili, M., Casini, P., Morelli, L. and Vestroni, F.: Vibration mitigation of rail noise barriers by hysteretic absorbers. J. Appl. Comput. Mech. (2020)
55. Vestroni, F., Casini, P.: Mitigation of structural vibrations by hysteretic oscillators in internal resonance. Nonlinear Dyn. **99**(1), 505–518 (2020)

56. Lacarbonara, W., Cetraro, M.: Flutter control of a lifting surface via visco-hysteretic vibration absorbers. Int. J. Aeronaut. Space Sci. **12**(4), 331–345 (2011)
57. Malher, A., Touzé, C., Doaré, O., Habib, G., Kerschen, G.: Flutter control of a two-degrees-of-freedom airfoil using a nonlinear tuned vibration absorber. J. Comput. Nonlinear Dyn. **12**(5), 2017.
58. Arena, A., Taló, M., Snyder, M.P., Lacarbonara, W.: Enhancing flutter stability in nanocomposite thin panels by harnessing CNT/polymer dissipation. Mech. Res. Commun. **104**, p. 103495 (2020).
59. Strganac, T.W., Ko, J., Thompson, D.E., Kurdila, A.J.: Identification and control of limit cycle oscillations in aeroelastic systems. J. Guid. Control. Dyn. **23**(6), 1127–1133 (2000)
60. Nayfeh, A.H., Balachandran, B.: Applied nonlinear dynamics. J. Wiley & Sons, New York (1995)
61. Nayfeh, A.H.: Introduction to perturbation techniques. Wiley Series in Nonlinear Sceince, NY (1993)
62. Nayfeh, A.H.: The method of normal forms. Wiley-VCH, Weinheim (2011)
63. Pettit, C.L., Beran, P.S.: Effects of parametric uncertainty on airfoil limit cycle oscillation. J. Aircraft **40**(5) (2003).